# *Gaia* photometry for white dwarfs[*]

J. M. Carrasco[1], S. Catalán[2,4], C. Jordi[1], P.-E. Tremblay[3], R. Napiwotzki[4], X. Luri[1], A.C. Robin[5], and P. M. Kowalski[6]

[1] Departament d'Astronomia i Meteorologia, Institut del Ciències del Cosmos (ICC), Universitat de Barcelona (IEEC-UB), c/ Martí i Franquès, 1, 08028 Barcelona, Spain, e-mail: `carrasco@am.ub.es`, `carme@am.ub.es`, `xluri@am.ub.es`

[2] Department of Physics, University of Warwick, Gibbet Hill Road, Coventry, CV4 7AL, UK, e-mail: `s.catalan-ruiz@warwick.ac.uk`

[3] Hubble Fellow, Space Telescope Science Institute, 700 San Martin Drive, Baltimore, MD, 21218, USA, e-mail: `tremblay@stsci.edu`

[4] Centre for Astrophysics Research, University of Hertfordshire, Hatfield, AL10 9AB, UK, e-mail: `r.napiwotzki@herts.ac.uk`

[5] Université de Franche-Comté, Institut Utinam, UMR CNRS 6213, OSU Theta, BP1615, 25010 Besançon Cedex, France, e-mail: `annie@obs-besancon.fr`

[6] Institute of Energy and Climate Research (IEK-6), Forschungszentrum Jülich, 52425 Jülich, Germany, e-mail: `p.kowalski@fz-juelich.de`

March 24, 2014, Received / Accepted

**ABSTRACT**

*Context.* White dwarfs can be used to study the structure and evolution of the Galaxy by analysing their luminosity function and initial mass function. Among them, the very cool white dwarfs provide the information for the early ages of each population. Because white dwarfs are intrinsically faint only the nearby ($\sim 20$ pc) sample is reasonably complete. The *Gaia* space mission will drastically increase the sample of known white dwarfs through its 5–6 years survey of the whole sky up to magnitude $V = 20$–$25$.

*Aims.* We provide a characterisation of *Gaia* photometry for white dwarfs to better prepare for the analysis of the scientific output of the mission. Transformations between some of the most common photometric systems and *Gaia* passbands are derived. We also give estimates of the number of white dwarfs of the different galactic populations that will be observed.

*Methods.* Using synthetic spectral energy distributions and the most recent *Gaia* transmission curves, we computed colours of three different types of white dwarfs (pure hydrogen, pure helium, and mixed composition with H/He= 0.1). With these colours we derived transformations to other common photometric systems (Johnson-Cousins, Sloan Digital Sky Survey, and 2MASS). We also present numbers of white dwarfs predicted to be observed by *Gaia*.

*Results.* We provide relationships and colour-colour diagrams among different photometric systems to allow the prediction and/or study of the *Gaia* white dwarf colours. We also include estimates of the number of sources expected in every galactic population and with a maximum parallax error. *Gaia* will increase the sample of known white dwarfs tenfold to about 200 000. *Gaia* will be able to observe thousands of very cool white dwarfs for the first time, which will greatly improve our understanding of these stars and early phases of star formation in our Galaxy.

**Key words.** Stars: evolution, white dwarfs; Instrumentation: photometers; Space vehicles: instruments; Techniques: photometric; Galaxy: general; Photometry, UBVRI ; Photometry, ugriz

## 1. Introduction

White dwarfs (WDs) are the final remnants of low- and intermediate-mass stars. About 95% of the main-sequence (MS) stars will end their evolutionary pathways as WDs and, hence, the study of the WD population provides details about the late stages of the life of the vast majority of stars. Their evolution can be described as a simple cooling process, which is reasonably well understood (Salaris et al. 2000; Fontaine et al. 2001). WDs are very useful objects to understand the structure and evolution of the Galaxy because they have an imprinted memory of its history (Isern et al. 2001; Liebert et al. 2005). The WD luminosity function (LF) gives the number of WDs per unit volume and per bolometric magnitude (Winget et al. 1987; Isern et al. 1998). From a comparison of observational data with theoretical LFs important information on the Galaxy (Winget et al. 1987)

can be obtained (for instance, the age of the Galaxy, or the star formation rate). Moreover, the initial mass function (IMF) can be reconstructed from the LF of the relic WD population, that is, the halo/thick disc populations. The oldest members of these populations are cool high-mass WDs, which form from high-mass progenitors that evolved very quickly to the WD stage.

Because most WDs are intrinsically faint, it is difficult to detect them, and a complete sample is currently only available at very close distances. Holberg et al. (2008) presented a (probably) complete sample of local WDs within 13 pc and demonstrated that the sample becomes incomplete beyond that distance. More recently, Giammichele et al. (2012) provided a nearly complete sample up to 20 pc. Completeness of WD samples beyond 20 pc is still very unsatisfactory even though the number of known WDs has considerably increased thanks to several surveys. For instance, the Sloan Digital Sky Survey (SDSS), with a limiting magnitude of $g' = 19.5$ (Fukugita et al. 1996) and covering a quarter of the sky, has substantially increased the number

---

of spectroscopically confirmed WDs[1]. This has allowed several statistical studies (Eisenstein et al. 2006), and the consequent improvement of the WD LF and WD mass distribution (Kleinman et al. 2013; Tremblay et al. 2011; Krzesinski et al. 2009; De Gennaro et al. 2008; Hu et al. 2007; Harris et al. 2006). However, the number of very cool WDs and known members of the halo population is still very low. A shortfall in the number of WDs below $\log(L/L_\odot) = -4.5$ because of the finite age of the Galactic disc, called luminosity cut-off, was first observed in the eighties (e.g. Liebert 1980; Winget et al. 1987). The *Gaia* mission will be extremely helpful in detecting WDs close to the luminosity cut-off and even fainter, which is expected to improve the accuracy of the age determined from the WD LF.

*Gaia* is the successor of the ESA Hipparcos astrometric mission (Bonnet et al. 1997) and increases its capabilities drastically, both in precision and in number of observed sources, offering the opportunity to tackle many open questions about the Galaxy (its formation and evolution, as well as stellar physics). *Gaia* will determine positions, parallaxes, and proper motions for a relevant fraction of stars ($10^9$ stars, $\sim 1\%$ of the Galaxy). This census will be complete for the full sky up to $V = 20 - 25$ mag (depending on the spectral type) with unprecedented accuracy (Perryman et al. 2001, Prusti 2011). Photometry and spectrophotometry will be obtained for all the detected sources, while radial velocities will be obtained for the brightest ones (brighter than about 17th magnitude). Each object in the sky will transit the focal plane about 70 times on average.

The *Gaia* payload consists of three instruments mounted on a single optical bench: the astrometric instrument, the spectrophotometers, and one high-resolution spectrograph. The astrometric measurements will be unfiltered to obtain the highest possible signal-to-noise ratio. The mirror coatings and CCD quantum efficiency define a broad (white-light) passband named $G$ (Jordi et al. 2010). The basic shape of the spectral energy distribution (SED) of every source will be obtained by the spectrophotometric instrument, which will provide low-resolution spectra in the blue (330–680 nm) and red (640–1000 nm), BP and RP spectrophotometers, respectively (see Jordi et al. 2010, for a detailed description). The BP and RP spectral resolutions are a function of wavelength. The dispersion is higher at short wavelengths. Radial velocities will also be obtained for more than 100 million stars through Doppler-shift measurements from high-resolution spectra ($R \sim 5000$–$11\,000$) obtained in the region of the IR Ca triplet around 860 nm by the Radial Velocity Spectrometer (RVS). Unfortunately, most WDs will show only featureless spectra in this region. The only exception are rare subtypes that display metal lines or molecular carbon bands (DZ, DQ, and similar).

The precision of the astrometric and photometric measurements will depend on the brightness and spectral type of the stars. At $G = 15$ mag the end-of-mission precision in parallaxes will be $\sim 25\,\mu$as. At $G = 20$ mag the final precision will drop to $\sim 300\,\mu$as, while for the brightest stars ($6 < G < 12$ mag) it will be $\sim 10\,\mu$as. The end-of-mission $G$-photometric performance will be at the level of millimagnitudes. For radial velocities the precisions will be in the range 1 to 15 km s$^{-1}$ depending on the brightness and spectral type of the stars (Katz et al. 2011). For a detailed description of performances see the *Gaia* website[2].

An effective exploitation of this information requires a clear understanding of the potentials and limitations of *Gaia* data. This paper aims to provide information to researchers on the WD field to obtain the maximum scientific gain from the *Gaia* mission.

Jordi et al. (2010) presented broad *Gaia* passbands and colour-colour relationships for MS and giant stars, allowing the prediction of *Gaia* magnitudes and uncertainties from Johnson-Cousins (Bessell 1990) and/or SDSS (Fukugita et al. 1996) colours. That article used the BaSeL-3.1 (Westera et al. 2002) stellar spectral library, which includes SEDs with $-1.0 < \log g < 5.5$, and thus excluded the WD regime ($7.0 < \log g < 9.0$). The aim of the present paper is to provide a similar tool for characterizing *Gaia* observations of WDs. For that purpose, we used the most recent WD synthetic SEDs (Kilic et al. 2009b, 2010a; Tremblay et al. 2011; Bergeron et al. 2011, see Sect. 2) with different compositions to simulate *Gaia* observations. In Sect. 3 we describe the conditions of WD observations by *Gaia* (the obtained *Gaia* spectrophotometry, the WD limiting distances, expected error in their parallaxes, etc.). In Sect. 4 we provide the colour-colour transformations between *Gaia* passbands and other commonly used photometric systems like the Johnson-Cousins (Bessell 1990), SDSS (Fukugita et al. 1996), and 2MASS (Cohen et al. 2003). In Sect. 5 relationships among *Gaia* photometry and atmospheric parameters are provided. Estimates of the number of WDs that *Gaia* will potentially observe based on simulations by Napiwotzki (2009) and *Gaia* Universe Model Snapshot (GUMS, Robin et al. 2012) are provided in Sect. 6. Finally, in Sect. 7 we finish with a summary and conclusions.

## 2. Model atmospheres

To represent the SED of WDs, we used grids of pure hydrogen (pure-H), pure helium (pure-He), and also mixed-composition models (H/He= 0.1) with $7.0 < \log g < 9.0$ in steps of 0.5 dex. These SEDs were computed from state-of-the-art model atmospheres and were verified in recent photometric and spectral analyses of WDs (Kilic et al. 2009b, 2010a; Tremblay et al. 2011; Bergeron et al. 2011).

The pure-H models are drawn from Tremblay et al. (2011) and cover the range[3] of 1500 K $< T_{\rm eff} <$ 140 000 K. These models were recently improved in the cool-temperature regime with updated collision-induced absorption (CIA) opacities (see the discussion in Tremblay & Bergeron 2007). In the present paper we also account for the opacity generated by the red wing of Lyman-$\alpha$ computed by Kowalski & Saumon (2006). This opacity significantly changes the predicted flux in the $B$ passband at very cool temperatures ($T_{\rm eff} \lesssim 6000$ K). Models with this opacity source have been successful in reproducing SEDs of many cool WDs (Kowalski & Saumon 2006; Kilic et al. 2009a,b, 2010b; Durant et al. 2012). The colours for these improved models are accessible from Pierre Bergeron's webpage[4]. In Fig. 1, we compare the predicted spectra of cool (4000 K) pure-H atmosphere WDs using the former grid of Tremblay et al. (2011) with the present grid taking into account the Lyman-$\alpha$ opacity.

---

[1] SDSS catalogue from Eisenstein et al. (2006) added 9316 WDs to the 2249 WDs in McCook & Sion (1999). A more recent publication (Kleinman et al. 2013), using data from DR7 release, almost doubles that amount, with of the order of 20 000 WDs.

[2] http://www.cosmos.esa.int/web/gaia/science-performance

[3] The temperature steps for the Tremblay et al. (2011) grid are $\Delta T_{\rm eff} =$ 250 K for $T_{\rm eff} < 5500$ K, $\Delta T_{\rm eff} = 500$ K for 6000 K $< T_{\rm eff} < 17\,000$ K, $\Delta T_{\rm eff} = 5000$ K for 20 000 K $< T_{\rm eff} < 90\,000$ K, and $\Delta T_{\rm eff} = 10\,000$ K for $T_{\rm eff} > 90\,000$ K.

[4] http://www.astro.umontreal.ca/ bergeron/CoolingModels/
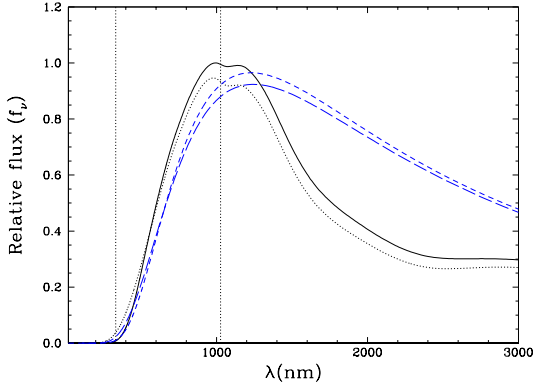
**Fig. 1.** Comparison of model SEDs with $T_{eff}$ = 4000 K and $\log g$ = 8.0. The pure-H models (in black) are computed with and without the Lyman-$\alpha$ opacity (solid and dotted lines). The pure-He models (in blue) are drawn from the sequence using the equation of state of Bergeron et al. (1995) and using the improved high-density physics of Kowalski et al. 2007 (medium and long dashed lines). The dotted vertical lines show the limits where the *Gaia* transmission is higher than 5%.



**Fig. 2.** $(G - V)$ vs. $T_{eff}$ diagram for WD SEDs (red filled squares and black opened circles) compared with pure-H SEDs without the Lyman-$\alpha$ opacity (blue filled circles) and pure-He SEDs from Kowalski et al. 2007 (green star symbols).

We additionally used pure-He models drawn from Bergeron et al. (2011), which cover a range[5] of 3500 K < $T_{eff}$ < 40 000 K. The cooler pure-He DC[6] models are described in more detail in Kilic et al. (2010a), and their main feature is the non-ideal equation of state of Bergeron et al. (1995). In recent years, new pure-He models of Kowalski et al. (2007), which include improved description of non-ideal physics and chemistry of dense helium, have also been used in the analysis of the data (Kilic et al. 2009b). These models include a number of improvements in the description of pure-He atmospheres of very cool WDs. These include refraction (Kowalski & Saumon 2004), non-ideal chemical abundances of species, and improved models of Rayleigh scattering and He⁻ free-free opacity (Iglesias et al. 2002; Kowalski et al. 2007). The SEDs of pure-He atmospheres are close to those of black bodies, since the He⁻ free-free opacity, which has a low dependence on wavelength, becomes the dominant opacity source in these models. In Fig. 1, we also present models at 4000 K drawn from the two pure-He sequences. The blue flux in Kowalski et al. (2007) is slightly higher than in Bergeron et al. (1995) since the contribution of the Rayleigh scattering is diminished. Note that the IR wavelength domain, which is not covered by *Gaia* detectors, is the range in which larger differences between the pure-H or pure-He composition are present. These differences result from strong CIA absorption by molecular hydrogen in hydrogen-dominated atmospheres.

Figure 2 shows that in spite of the different physics present in all these models, the colours (e.g. $G - V$) look quite similar for the different SED libraries. For this reason, and because the purpose of this paper is not to discuss the differences among the WD SED libraries, but to provide a way to predict how WDs will be observed by *Gaia*, in Sect. 4 we only included the transformations derived using one sequence for each composition (Tremblay et al. 2011 with Lyman-$\alpha$ for pure-H and Bergeron et al. 2011 for pure-He).

---

[5] The temperature steps for the Bergeron et al. (2011) grid are $\Delta T_{eff}$ = 250 K for $T_{eff}$ < 5500 K, $\Delta T_{eff}$ = 500 K for 6000 K < $T_{eff}$ < 10 000 K and $\Delta T_{eff}$ = 1000 K for $T_{eff}$ > 10 000 K.

[6] DC are WDs with featureless continuous spectra, which can have a pure-H, pure-He, or mixed atmosphere composition.
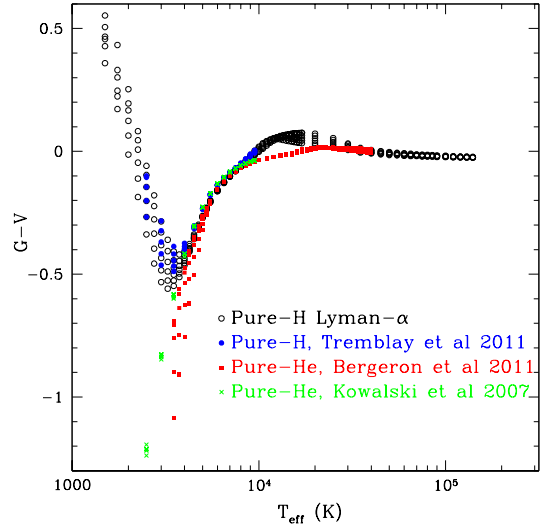
The mixed model atmospheres used here cover a range of 2500 K < $T_{eff}$ < 6000 K and are taken from Kilic et al. (2010a). In the following, we use an abundance ratio of H/He = 0.1 as a typical example for the composition of known mixed WDs (Kilic et al. 2009b, 2010a; Leggett et al. 2011; Giammichele et al. 2012). It has to be kept in mind that because of the nature of the CIA opacities, which are dominant in the near-IR and IR in this mixed regime, the predicted spectra can vary considerably for different H/He ratios with the same $T_{eff}$ and $\log g$ (see Fig. 10 of Kilic et al. 2010a). The colour space covered by our H/He = 0.1 sequence and the pure-H and He sequences illustrates the possible colour area where mixed-composition WDs can be found.

## 3. WDs as seen by *Gaia*

In Fig. 3 the synthetic SEDs of selected WDs (see Sect. 2) are shown together with the transmission curves of the $G$ passband, BP/RP spectrophotometry, and RVS spectroscopy. Low-resolution BP/RP spectra as will be obtained by *Gaia* for pure-H WDs are shown in Fig. 4. If these spectra are re-binned, summing all their pixels together, we obtain their corresponding magnitudes, $G_{BP}$, $G_{RP}$, and $G_{RVS}$ (Fig. 3). In the same way, we can reproduce any other synthetic passband, if needed (e.g. Johnson-Cousins, SDSS, or 2MASS, etc.).

The faint *Gaia* limiting magnitude will guarantee the detection of very cool WDs. In Table 1 we compute the maximum distances at which WDs with different temperatures and gravities will be detected with *Gaia*. Two limiting distances are provided, without considering interstellar absorption, $d$, and assuming an average absorption of 1 mag per kpc, $d_{A_V}$, corresponding to an observation made in the direction of the Galactic disc (O'Dell & Yusef-Zadeh 2000). We also provide the absolute magnitudes ($M_G$) and consider two different compositions, pure-H and pure-He. All WDs with $T_{eff}$ > 20 000 K will be detected within 270 pc and all with $T_{eff}$ > 10 000 K within 150 pc, regardless of the atmospheric composition or interstellar absorption. The brightest unreddened WDs will even be observed farther away than 1.5 kpc. For the coolest regime the space volume of observation is

**Table 1.** Maximum distances, $d$, at which unreddened WDs will be observed by *Gaia* for pure-H (Tremblay et al. 2011) and pure-He (Bergeron et al. 2011, which only covers $T_{eff} > 3500$ K) models. $d_{A_V}$ is the limiting distance when an average reddening corresponding to an observation in the disc direction has been applied (assuming an extinction of 1 mag·kpc$^{-1}$). The ages of all these WDs can be consulted in the CDS online tables (Tables 3 – 5). $M_G$ is the absolute magnitude at $G$ passband.

| $T_{eff}$ | $\log g = 7.0$ | | | $\log g = 8.0$ | | | $\log g = 9.0$ | | |
|---|---|---|---|---|---|---|---|---|---|
| | $M_G$ | $d$ (pc) | $d_{A_V}$ (pc) | $M_G$ | $d$ (pc) | $d_{A_V}$ (pc) | $M_G$ | $d$ (pc) | $d_{A_V}$ (pc) |
| Pure-H (Lyman-$\alpha$) | | | | | | | | | |
| 2000 | 17.28 | 35 | 34 | 18.22 | 23 | 22 | 19.77 | 11 | 11 |
| 3000 | 15.80 | 69 | 67 | 16.76 | 45 | 44 | 18.38 | 21 | 21 |
| 4000 | 14.86 | 107 | 102 | 15.84 | 68 | 66 | 17.44 | 33 | 32 |
| 5000 | 13.72 | 180 | 167 | 14.86 | 107 | 102 | 16.55 | 49 | 48 |
| 10 000 | 10.74 | 711 | 552 | 12.18 | 366 | 317 | 13.96 | 161 | 151 |
| 20 000 | 9.23 | 1425 | 929 | 10.81 | 689 | 538 | 12.59 | 303 | 268 |
| Pure-He | | | | | | | | | |
| 4000 | 15.16 | 93 | 89 | 16.09 | 61 | 59 | 17.77 | 28 | 27 |
| 5000 | 13.76 | 177 | 164 | 14.86 | 107 | 102 | 16.58 | 48 | 47 |
| 10 000 | 10.92 | 655 | 516 | 12.28 | 350 | 304 | 14.02 | 157 | 147 |
| 20 000 | 9.17 | 1465 | 947 | 10.68 | 731 | 564 | 12.44 | 325 | 285 |
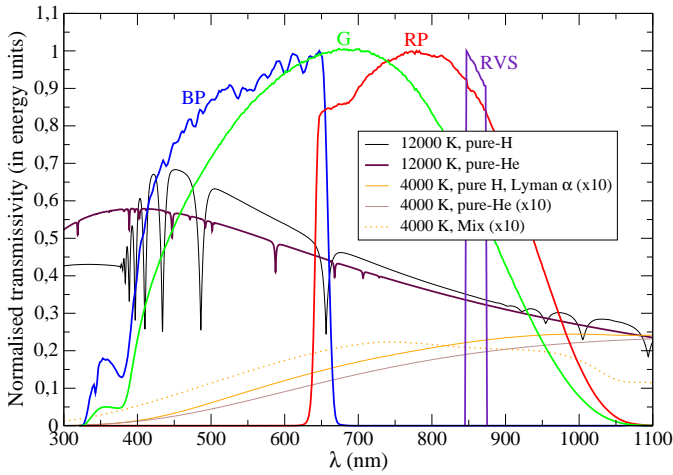


**Fig. 3.** *Gaia* passbands transmissivity. $G$ passband is depicted in green, $G_{BP}$ in blue, $G_{RP}$ in red, and $G_{RVS}$ in magenta lines. All WD SEDs plotted here (described in Sect. 2) correspond to $\log g = 8.0$.
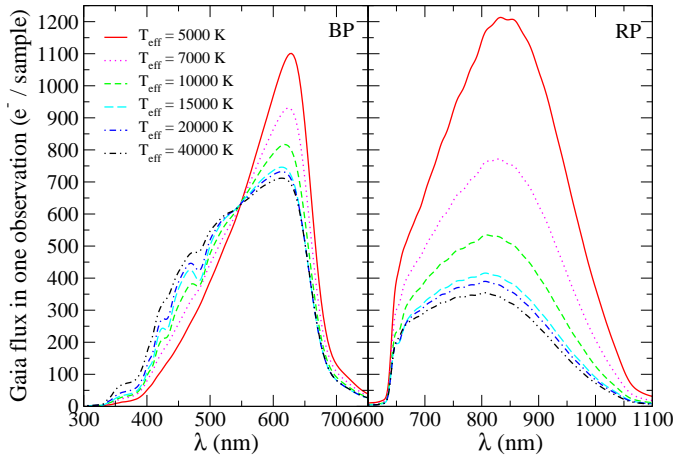


**Fig. 4.** Examples of *Gaia* BP/RP spectra for pure-H WDs (Tremblay et al. 2011) with different temperatures at $G = 15$ mag. All SEDs plotted here have $\log g = 8.0$.
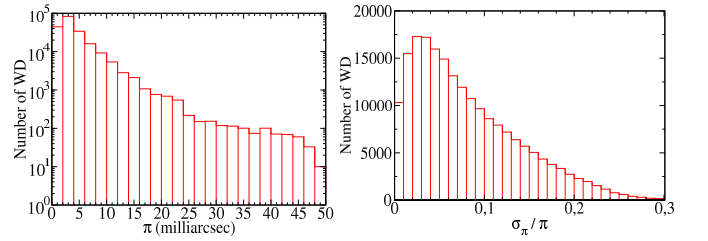


**Fig. 5.** Histogram of parallaxes (left) of single WDs with $G \leq 20$ using data from GUMS. Histogram of parallax relative errors (right) computed using *Gaia* performances[2].

will provide precise locations in the Hertzsprung–Russell (HR) diagrams (see Sect. 5). Estimates of the number of WDs observed by *Gaia* with a given parallax and a given relative error in the parallax are provided in Fig. 5 (left and right, respectively), based on simulations performed with GUMS, see Sect. 6. The errors in parallaxes were computed using *Gaia* performance prescriptions[2]. Estimates derived from Fig. 5 of the number of WDs with better parallax precision than a certain threshold are provided in the upper part of Table 2. About 95% of the isolated WDs brighter than $G = 20$ will have parallaxes more precise than 20%.

Expected end-of-mission parallax uncertainties were also computed for two observational datasets extracted from SDSS data. The first sample includes 125 cool ($T_{eff} < 7000$ K) WDs analysed by Kilic et al. (2010a), the second data set includes almost 3000 hot (6000 K $< T_{eff} <$ 140 000 K), non-magnetic and single WDs from Tremblay et al. (2011). The relative error of their parallaxes, derived from predicted distances, are shown in Fig. 6. For these samples, we computed the values quoted in the bottom part of Table 2. As can be seen, 94% of the WDs will have parallax determinations better than 10%, corresponding to absolute magnitudes with uncertainties below 0.2 mag, which allows a clear distinction between WDs and MS stars. While the masses for the sample of Tremblay et al. (2011) are known from spectroscopic fits, the masses of the cool WDs from Kilic et al. (2010a) are not constrained, and therefore *Gaia* will be able to provide this information for the first time.

*Gaia* will also observe (and discover new) binaries containing WDs (according to simulations by GUMS shown in Table 9, only 36% of WDs detected by *Gaia* will be single) and orbital solutions will be achieved for a significant number of them.

smaller, especially at high $\log g$, with detections restricted to the nearest 50 pc (for $T_{eff} = 5000$ K).

The *Gaia* photometry combined with its extremely precise parallaxes will allow absolute magnitudes to be derived, which

**Table 2.** Approximate number of WDs (all temperatures) with parallaxes better than a certain percentage, derived using the GUMS dataset and real WD SDSS datasets (extracted from Kilic et al. 2010a; Tremblay et al. 2011).

| | GUMS | | | |
|---|---|---|---|---|
| | All WDs | | Single WDs | |
| $\sigma_\pi / \pi$ | $N$ | % of observed | $N$ | % of observed |
| ≤1% | 20 000 | 3.5% | 10 000 | 5% |
| ≤5% | 150 000 | 25% | 75 000 | 40% |
| ≤10% | 300 000 | 50% | 135 000 | 70% |
| ≤20% | 450 000 | 80% | 190 000 | 95% |
| | WDs from SDSS samples | | | |
| | Kilic et al. (2010a) | | Tremblay et al. (2011) | |
| $\sigma_\pi / \pi$ | $N$ | % of observed | $N$ | % of observed |
| ≤1% | 76 | 61% | 500 | 16% |
| ≤5% | 125 | 100% | 2275 | 74% |
| ≤10% | 125 | 100% | 2880 | 94% |
| ≤20% | 125 | 100% | 3048 | 99% |
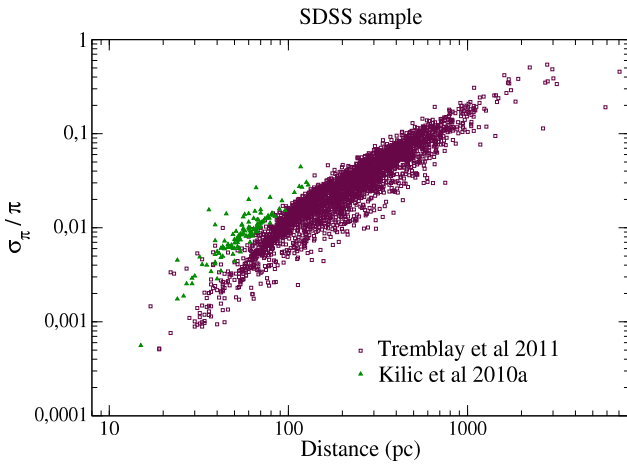


**Fig. 6.** Relative error in *Gaia* parallax as a function of the distance for real WDs observed by SDSS, showing that *Gaia* will be precise enough to easily cover the 100 pc WD sample at a ~ 1% level.

Therefore, *Gaia* will provide independent mass determinations of WDs. These data are desirable to check and calibrate the currently available mass estimates of WDs based on the models and photometric/spectroscopic data. Among all these binaries, eclipsing binaries will be extremely useful to determine the radius of the WD. We currently know more than 2000 binary pairs composed of a WD and an MS star (Rebassa-Mansergas et al. 2011). Only 34 systems of this sample are eclipsing binaries. About a thousand more will be discovered by *Gaia*.

## 4. *Gaia* photometric transformations

For each available WD SED in the libraries described in Sect. 2, we computed their *Gaia* photometry as they would be observed with *Gaia* and other commonly used photometric systems (Johnson-Cousins, SDSS and 2MASS) following the same strategy as Jordi et al. (2010). The results are listed in the CDS online Tables 3 – 5. The contents of these tables include the astrophysical parameters of the WDs (effective temperature, surface gravity, mass in solar masses, bolometric magnitude, bolometric correction in $V$, and age) as well as their simulated absolute magnitudes in Johnson-Cousins ($U$, $B$, $V$, $R_C$, $I_C$), 2MASS ($J$, $H$,

$K_S$), SDSS ($u$, $g$, $r$, $i$, $z$), and *Gaia* passbands ($G$, $G_{BP}$, $G_{RP}$, and $G_{RVS}$). The three different tables correspond to different compositions of the WDs (pure-H in Table 3, pure-He in Table 4, and mixed composition with H/He=0.1 in Table 5).

Because WDs are intrinsically faint objects, they are observed close to us. Because of this, they are not much affected by extinction[7]. For this reason, the colour transformations presented in this section were obtained without reddening effects, which are considered negligible for most WDs observed by *Gaia*. The hot WDs in the Galactic disc direction may, however, suffer from mild to considerable reddening, although this will have to be studied on a case-by-case basis, which is currently beyond the scope of this work.

### 4.1. Johnson-Cousins and SDSS colours

Figures 7–8 show several colour-colour diagrams relating *Gaia*, Johnson-Cousins (Bessell 1990), and SDSS passbands (Fukugita et al. 1996). Only 'normal' pure-H ($T_{eff} > 5000$ K) and pure-He composition WDs are plotted. In this range of $T_{eff}$, colours of mixed composition WDs coincide with those of pure-H WDs and are not overplotted for clarity. The relationship among colours is tight for each composition, that is, independent of the gravities. However, the $B$ and to a lesser degree the $V$ passband induce a distinction between the pure-H and the pure-He WDs at $T_{eff} \sim 13\,000$ K, where the Balmer lines and the Balmer jump are strong in pure-H WDs.

Synthetic photometry was also computed for 82 real WDs extracted from the list of Pancino et al. (2012). They are SpectroPhotometric Standard Star (SPSS) candidates for the absolute flux calibration of *Gaia* photometric and spectrophotometric observations. The whole list of SPSS is selected from calibration sources already used as flux standards for HST (Bohlin 2007), some sources from CALSPEC standards (Oke 1990, Hamuy et al. 1992, Hamuy et al. 1994, Stritzinger et al. 2005), and finally McCook & Sion (1999) but also SDSS, and other sources. The colours computed with the SEDs of the libraries used here (Sect. 2) agree very well with those of SPSS true WDs.

Because of the very tight relationship among colours, polynomial expressions were fitted. 240 synthetic pure-He and 276 synthetic pure-H WDs were used for the fitting. We provide the coefficients for third-order polynomials and the dispersion values in Table 6 (available online). Table 6 contains the following information. Column 1 lists the name of the source, Column 2 gives the bolometric luminosity, etc.

The dispersions are smaller than 0.02 mag for the SDSS passbands, while for the Johnson-Cousins passbands they can reach 0.06 mag in some case, mainly for pure-H and when blue $B$ or $G_{BP}$ passbands are involved. The expressions presented here are useful to predict *Gaia* magnitudes for WDs of different $T_{eff}$ and atmospheric compositions, for which colours in the Johnson-Cousins photometric system are known. These expressions should only be used in the $T_{eff}$ regimes indicated in Table 6. In all other cases, individual values from the CDS online Tables 3–5 can be used instead.

In the cool regime, $T_{eff} < 5000$ K, and for pure-H composition the colours depend considerably on the surface gravity, yielding a spread in the colour-colour diagrams (see Figs. 9 and 10). Therefore, no attempt has been made to include these cool pure-H WDs into the computation of the polynomial transformations. To derive the *Gaia* magnitudes, we recommend the use

[7] The most reddened observable WDs in Table 1 have $A_V < 1$ mag, assuming an extinction of 1 mag·kpc$^{-1}$.

5
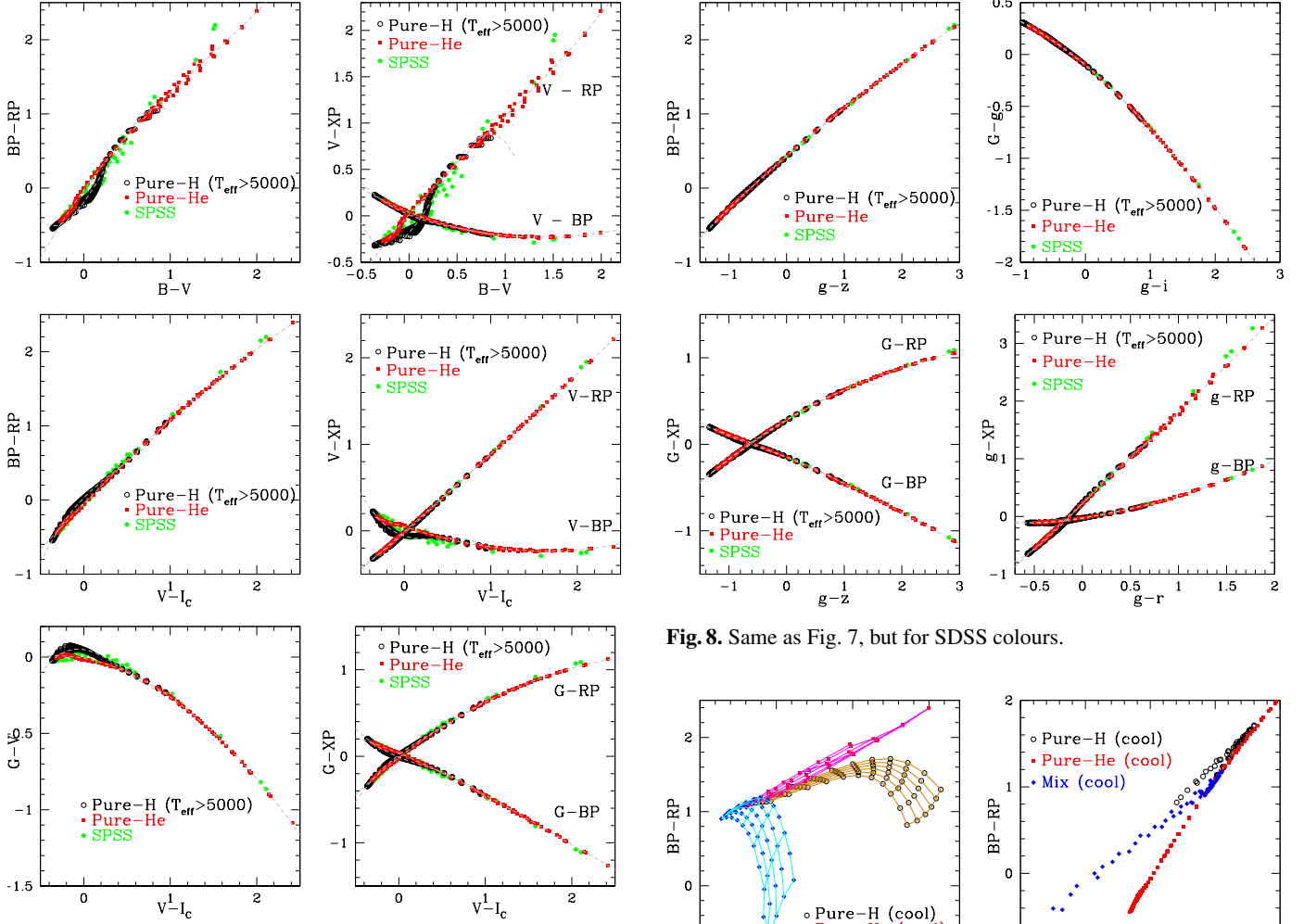
**Fig. 7.** Several colour-colour diagrams obtained using *Gaia* and Johnson-Cousins passbands for the 'normal' regime of pure-H ($T_{eff} > 5000$ K; black open circles) and for pure-He (red squares) WDs. Green star symbols correspond to real WDs selected from Pancino et al. (2012). Grey dashed curves are the fitted polynomials from Table 6.

of the individual values for the desired temperature and surface gravity listed in the CDS online Tables 3 − 5.

### 4.2. 2MASS colours

Figure 11 shows some of the diagrams combining *Gaia* and 2MASS (Cohen et al. 2003) colours, in this case including both 'normal' and cool WDs. The relationships are not as tight because *Gaia* and 2MASS passbands are sampling different wavelength ranges of the SED and the 2MASS near-IR regime is more sensitive to the composition of WDs than *Gaia*'s optical range (see Fig. 1). Table 7 (available online) provides the coefficients of third-order fittings for 'normal' pure-H with $T_{eff} > 5000$ K and pure-He WDs. The dispersion values are higher than for Johnson-Cousins or SDSS, as expected, and increase up to 0.1 mag in the worst cases. The user can employ the individual values for the desired temperature and surface gravity listed in the CDS online Tables 3 − 5 if the dispersion is too large.



**Fig. 8.** Same as Fig. 7, but for SDSS colours.
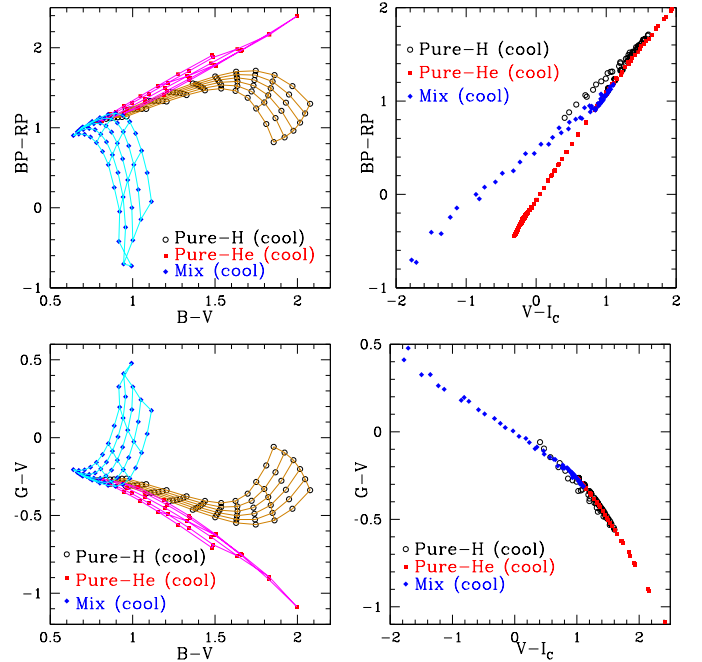


**Fig. 9.** Several colour-colour diagrams obtained using *Gaia* and Johnson-Cousins passbands in the cool regime ($T_{eff} < 5000$ K).

## 5. Classification and parametrisation

The spectrophotometric instrument onboard *Gaia* has been designed to allow the classification of the observed objects and their posterior parametrisation. The classification and parametrisation will be advantageous in front of other existing or planned photometric surveys because of the combination of spectrophotometric and astrometric *Gaia* capabilities. The extremely precise parallaxes will permit one to decontaminate the WD population from cool MS stars or subdwarfs. Parallaxes are especially important for very cool WDs ($T_{eff} < 5000$ K) since *Gaia*

**Fig. 10.** Same as Fig. 9, but for SDSS passbands.
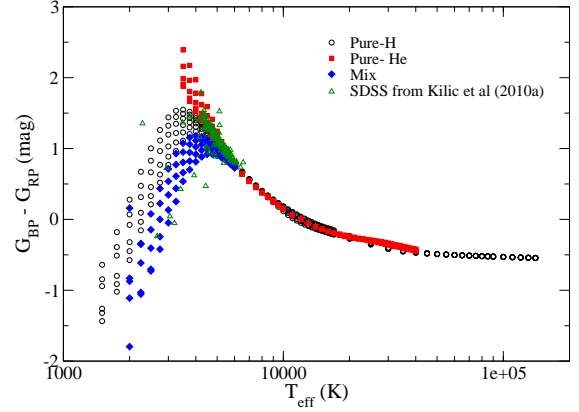


**Fig. 11.** Several colour-colour diagrams obtained using *Gaia* and 2MASS passbands for all $T_{eff}$.



**Fig. 12.** $G_{BP}$-$G_{RP}$ colour dependency with $T_{eff}$ for pure-H (black), pure-He (red), or mixed composition (blue) WDs. WDs observed by SDSS and included in Kilic et al. (2010a) are also plotted (in green).
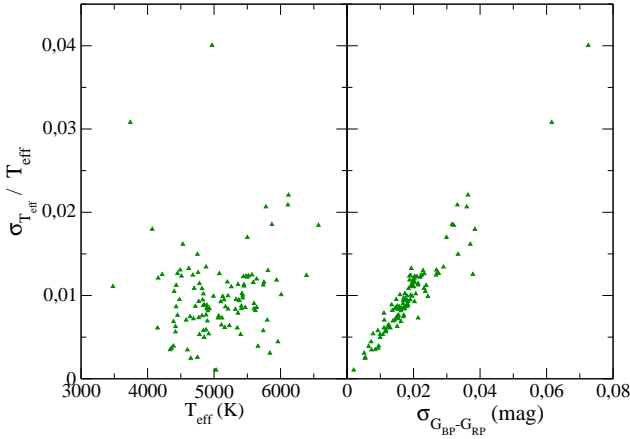
physical parameters of WDs, but just to provide some clues on how to obtain from *Gaia* the relevant information to derive the temperature, surface gravity, and composition of WDs.

**Effective temperature:** in Fig. 12, we can see the strong correlation between $G_{BP} - G_{RP}$ colour and $T_{eff}$ valid for all compositions when $T_{eff} > 5000$ K, while for the cool regime the colour-temperature relationship depends on the composition and the surface gravity. The flux depression in the IR due to CIA opacities in pure-H and mixed compositions causes that the relationship presents a turnaround at $G_{BP} - G_{RP} \sim 1.7$. WDs with $G_{BP} - G_{RP} > 1.7$ most likely have pure-He composition and $T_{eff} \sim 3000$–4000 K. Therefore, *Gaia* is expected to shed light on the atmospheric composition of the coolest WDs.

$G_{BP} - G_{RP}$ colours for the WDs observed by SDSS and included in Kilic et al. (2010a) have been computed from their $g - z$ colours using the polynomial expressions in Table 6 (available online) and are also included in Fig. 12 for comparison purposes. Assuming that a prior classification in the 'normal' or cool regime has been performed from parallax information, the $G_{BP} - G_{RP}$ vs $T_{eff}$ relationship can be used to derive temperatures. The slope of the relationship for pure-He WDs and the expected errors of $G_{BP} - G_{RP}$ (estimated from *Gaia* expected performances webpage[2]) were used to compute the $T_{eff}$ errors for the Kilic et al. (2010a) WDs (Fig. 13). From these SDSS WDs we found a mean $\sigma_{T_{eff}}/T_{eff}$ of $\sim 1\%$.

**Surface gravity:** the spectral region around $\lambda = 360$–500 nm with the hydrogen Balmer lines is particularly useful to derive the surface gravity. Although the transmission of $G_{BP}$ is low at this wavelength range, the end-of-mission signal-to-noise ratio is better than 15 for $G \leq 16.5$ (if $T_{eff} = 5000$ K) or even $G \leq 17.7$ (if $T_{eff} = 40\,000$ K). Unfortunately, it is doubtful that precise atmospheric parameters determination can be performed with *Gaia* BP/RP spectra alone because of the low resolution of the BP/RP instruments. We recall that by combining the *Gaia* parallaxes and magnitudes with $T_{eff}$ estimates as described above and a theoretical mass-radius relationship for WDs, it is possible to derive fairly precise $\log g$ values.

**Chemical composition:** the difference between pure-H and pure-He is visible in the Balmer jump (with a maximum around $T_{eff} \sim 13\,000$ K) and the analysis of BP/RP of WD spectra (not only their colours) will help to identify the dif-

will provide the necessary data to derive the masses of already known WDs (for the first time) and newly discovered cool WDs.

The classification and a basic parametrisation of the sources will be provided in the intermediate and final *Gaia* data releases in addition to the spectrophotometry and integrated photometry. This classification and parametrisation process will be performed by the *Gaia* Data Processing and Analysis Consortium, which is in charge of the whole data processing, and will be based on all astrometric, spectrophotometric, and spectroscopic *Gaia* data (Bailer-Jones et al. 2013). The purpose here is not to define or describe the methods to be used to determine the astro-

**Fig. 13.** Relative error in $T_{eff}$ derived for real WDs observed by SDSS and extracted from Kilic et al. (2010a) as a function of $T_{eff}$ (left) and of the uncertainty in *Gaia* $G_{BP} - G_{RP}$ colour (right).

ferences in composition (see Fig. 3). However, to determine atmospheric parameters, it will be better to use *Gaia* photometry constrained by the parallax information. Additional observations may be necessary to achieve a better accuracy on the atmospheric parameters, such as additional photometry or higher resolution spectroscopic follow-up. A comparison of the masses obtained from the *Gaia* parallaxes with those determined from spectroscopic follow-up will allow one to test the mass-radius relations and the internal chemical composition for WDs.

The *Gaia* RVS range around 860 nm is not optimal to see features in WD SEDs (only DZ and similar rare WDs with metal lines will show some features in this region). Ground-based follow-up spectroscopic observations around the hydrogen Balmer lines need to be obtained to derive radial velocities and abundances.

The SED of the pure-H and pure-He WDs differ considerably in the IR wavelength range, particularly in the cool domain (see Fig. 1), and thus, the combination of *Gaia* and IR photometry will allow one to disctinguish among compositions. Figure 11 shows *Gaia*−2MASS colour-colour diagrams. The all-sky 2MASS catalogue can be used for WDs brighter than $J = 16.5$, $H = 16.5$ and $K = 16$, which are the limiting magnitudes of the survey. *Gaia* goes much fainter, and therefore near-IR surveys such as the UKIDSS Large Area Survey ($J_{lim} = 20$, $K_{lim} = 18.4$, Hewett et al. 2006), VIKING (VISTA Kilo-Degree Infrared Galaxy Survey; $J_{lim} = 20.9$, Findlay et al. 2012), and VHS (VISTA Hemisphere Survey, $J_{lim} = 21.2$, Arnaboldi et al. 2010) will be of great interest, although they only cover 4000, 1500, and 20 000 deg², respectively.

## 6. White dwarfs in the Galaxy

The currently known population of WDs amounts to ∼ 20 000 objects (Kleinman et al. 2013). This census will be tremendously increased with the *Gaia* all-sky deep survey, and more significantly for the halo population and the cool regime (Torres et al. 2005). We present estimates of the number of WDs that will be observed (see Tables 9 – 10 and Figs. 14 – 17) according to two different simulations: one extracted from the *Gaia* Universe Model Snapshot (GUMS, Robin et al. 2012) and another one based on Napiwotzki (2009). These simulations (which only in-

clude pure-H WDs) were adapted to provide *Gaia* -observed samples (limited to $G = 20$). Both simulations build their stellar content based on the galactic structure in the Besançon Galaxy Model, (BGM, Robin et al. 2003), but some differences were considered in each simulation since then.

The BGM considers four different stellar populations: thin disc, thick disc, halo, and bulge, of which the latter has little relevance for our simulations and will thus not be discussed any further. An age-dependent scale height is adopted for the thin disc and both WD simulations assume a constant formation rate of thin-disc stars. The thick disc is modelled with a scale height of 800 pc, and the stellar halo as a flattened spheroid.

Although the ingredients of the simulations have been detailed in the original papers, we briefly summarize in Sects. 6.1 and 6.2 some relevant information for each simulation to help understand their compared results in Sect. 6.3.

### 6.1. Simulations using GUMS

GUMS provides the theoretical Universe Model Snapshot seen by *Gaia* and is being used for mission preparation and commissioning phases. It can be used to generate stellar catalogues for any given direction and returns information on each star, such as magnitude, colour, and distance, as well as kinematics and other stellar parameters. Although only WD simulations were extracted, GUMS also includes many Galactic and extra-galactic objects, and within the Galaxy it includes isolated, double, and multiple stars as well as variability and exoplanets. The ingredients of GUMS regarding the WD population are summarized here:

– Thin-disc WDs are modelled following the Fontaine et al. (2001) pure-H WD evolutionary tracks, assuming the Wood (1992) LF for an age of 10 Gyr and an IMF from Salpeter (1955). It has been normalised to provide the same number of WDs of $M_V \leq 13$ as derived by Liebert et al. (2005) from the Palomar Green Survey. The photometry was calculated by Bergeron et al. (2011).
– For the thick disc, the WD models of Chabrier (1999) were used assuming an age of 12 Gyr. For the normalisation, the ratio between the number of MS turn-off stars and the number of WDs depends on the IMF and on the initial-to-final mass relation, assuming that all stars with a mass greater than the mass at the turn-off ($M_{TO} = 0.83$ $M_\odot$) are now WDs. However, the predicted number of thick-disc WDs with this assumption is much higher than the number of observed WDs in the Oppenheimer et al. (2001) photographic survey of WDs. This led Reylé et al. (2001) to normalise the thick-disc WD LF to that of the Oppenheimer et al. (2001) sample, assuming it is complete: the ratio between the number of WDs (initial mass > 0.83 $M_\odot$) and the number of MS stars (initial mass < 0.83 $M_\odot$) is taken to be 20%.
  Because the completeness of the Oppenheimer et al. (2001) sample is not certain, this value can be considered as a lower limit. This normalisation also agrees with the number of WDs in the expanded Luyten half-second proper motion catalogue (LHS) WD sample (Liebert et al. 1999).
– The halo LF is derived from the truncated power-law initial mass function IMF2 of Chabrier (1999) with an age of 14 Gyr. It was specifically defined to generate a significant number of MACHOS in the halo to explain the number of microlensing events towards the Magellanic Clouds. Hence the density of halo WDs is assumed to be 2% of the density of the dark halo locally. Because of the assumed IMF, which

**Table 8.** Local densities used in both WD Galaxy simulations, expressed in $M_\odot \cdot pc^{-3}$.

|  | Napiwotzki (2009) | GUMS |
|---|---|---|
| Thin | $2.9 \cdot 10^{-3}$ | $4.16 \cdot 10^{-3}$ |
| Thick | $1.7 \cdot 10^{-3}$ | $5.06 \cdot 10^{-4}$ |
| Halo | $2.7 \cdot 10^{-4}$ | $2.80 \cdot 10^{-4}$ |

**Table 9.** Total number of WDs with $G \leq 20$ expected in *Gaia* for different $T_{eff}$ ranges.

| $T_{eff}$ | $N_{Thin}$ | $N_{Thick}$ | $N_{Halo}$ |
|---|---|---|---|
| Napiwotzki (2009) | | | |
| All range, single | 196 765 | 48 673 | 9705 |
| < 5000 K, single | 925 | 1883 | 347 |
| GUMS | | | |
| All range, single | 198 107 | 3557 | 63 |
| All range, Comp A | 64 905 | 2340 | 47 |
| All range, Comp B | 296 976 | 1153 | 4 |
| < 5000 K, single | 8845 | 142 | 63 |
| < 5000 K, Comp A | 862 | 95 | 47 |
| < 5000 K, Comp B | 244 | 12 | 4 |

**Table 10.** Number and types of variable WDs as predicted by GUMS.

| Variables | ZZCeti | Dwarf Novae | Classical Novae |
|---|---|---|---|
| Isolated | 18 363 | – | – |
| In binary | 6463 | 340 | 10 258 |

is highest at M = 2.4 $M_\odot$, the generated WDs have cooled down with an LF peaking at $M_V \approx 16.5-17$. Hence the number of halo WDs observable at $G < 20$ is rather small (see Table 9), despite their large local density. This is one of the main differences (see Sect. 6.3) with respect to simulations obtained with Napiwotzki (2009). The total local density for each population is included in Table 8.

– GUMS adopts the 3D extinction model by Drimmel et al. (2003).

### 6.1.1. Variable and binary WDs

– Several types of intrinsic stellar variability were considered, and for WDs, they include pulsation of ZZ-Ceti type, cataclysmic dwarfs, and classical novae types. For WDs in close-binary systems (period shorter than 14 hours), half of them are simulated as dwarf novae and the other half as classical novae. WD+WD close-binary systems are also considered in these simulations.

– Although the simulation of binaries is already quite realistic in GUMS, it still needs some further refinement in the specific case of WDs.

Work is on-going to improve the mass distribution in new versions of the *Gaia* simulator. For this reason, we are still unable to detail the number of WDs in binary systems in which orbital parameters can be obtained to provide independent mass estimates of the WDs. This study will be possible with future versions of the GUMS simulations.

### 6.2. Simulations using Napiwotzki (2009)

Napiwotzki (2009) used the Galactic model structure of BGM to randomly assign positions of a large number of stars based on observed densities of the local WD population. Depending on population membership, each star is given a metallicity, an initial mass, and kinematical properties. The ingredients are summarized in the following items:

– The WD cooling sequences were created by combining the tracks of Blöcker (1995) for hot WDs with the sequences of Fontaine et al. (2001) for cooler WDs.

– The WD progenitor lifetime was calculated from the stellar tracks of Girardi et al. (2000).

– The initial-final mass relationship by Weidemann (2000) was considered.

– The relative contributions of each Galactic population were calibrated using the kinematic study of Pauli et al. (2006) of the brightness-limited SPY (ESO SN Ia Progenitor Survey: Napiwotzki et al. 2001) sample. Pauli et al. (2006) assigned population membership according to a set of criteria based on the measured 3D space velocity. An iterative correction for mis-assignment of membership of WDs with ambiguous kinematic properties was derived from the model (see Napiwotzki 2009).

– Space densities were then calculated from the relative contributions and the WD numbers in the 13 pc sample of Holberg et al. (2008). The finally adopted local densities can be seen in Table 8.

– Holberg & Bergeron (2006) colour tables were used for WD simulations, and photometric transformation from Table 6 of the present paper were used to carry out the brightness selection for the *Gaia* sample.

– IMFs from Salpeter (1955) were used to derive numbers in Table 9, although other IMFs (e.g. Chabrier 1999; Baugh et al. 2005) were tested as well. These would give higher numbers of cool, high mass WDs.

Napiwotzki (2009) compared the simulations with the proper-motion-selected sample of Oppenheimer et al. (2001). Simulated numbers turned out to be slightly higher, which can easily be explained by a minor incompleteness of the observed sample.

### 6.3. Results

Table 9 shows the number of WDs detectable for each population (about 200 000–250 000 single WDs in total) according to the two simulations explained above. Table 10 shows the expected number and types of variable WDs observed by *Gaia*, according to GUMS.

Most of the observed WDs belong to the thin disc because of the still on-going star formation. The number of thin-disc WDs in the two simulations agree remarkably well at the level of 1% for single stars. We note that in GUMS binaries are added and produce about $3.6 \cdot 10^5$ additional thin-disc WDs (see Table 9). However, this estimate includes WDs in binary systems that are not resolvable by *Gaia* alone. Just for comparison, previous estimates of the number of WDs in the disc reported by Torres et al. (2005) provided $3.9 \cdot 10^5$ WDs with $G < 20$ mag.

The small number of WDs known in thick-disc and halo populations is the current limiting factor to constrain their properties. Due to these limitation, Napiwotzki (2009) and GUMS arrive at different interpretations of the Oppenheimer et al. (2001)

9
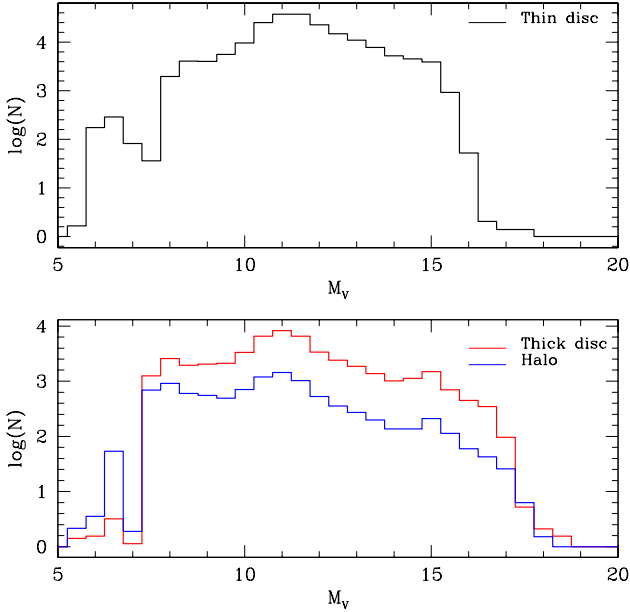
**Fig. 14.** Simulated *Gaia* $M_V$ distribution of a single WD population with $G < 20$ mag from thin-disc (top panel), thick-disc and halo populations (bottom panel) based on Napiwotzki (2009).



**Fig. 15.** Same as Fig. 14, now using GUMS simulations.

sample. The local thick-disc density assumed by Napiwotzki (2009) is three times higher than the one assumed by GUMS (see Table 8). The local densities for the halo are more similar, but the more stringent difference comes from the shapes of the assumed LF and the IMFs. The IMF assumed by GUMS leads to a very low estimated number of thick-disc and halo WDs observable by *Gaia*.

As expected, the number of observable cool WDs ($T_{eff} < 5000$ K) of all populations will be considerably smaller than the total sample. However, this will still represent a dramatic increase compared with any previous survey (e.g. only 35 cool WDs were found in the SDSS sample by Harris et al. 2006).

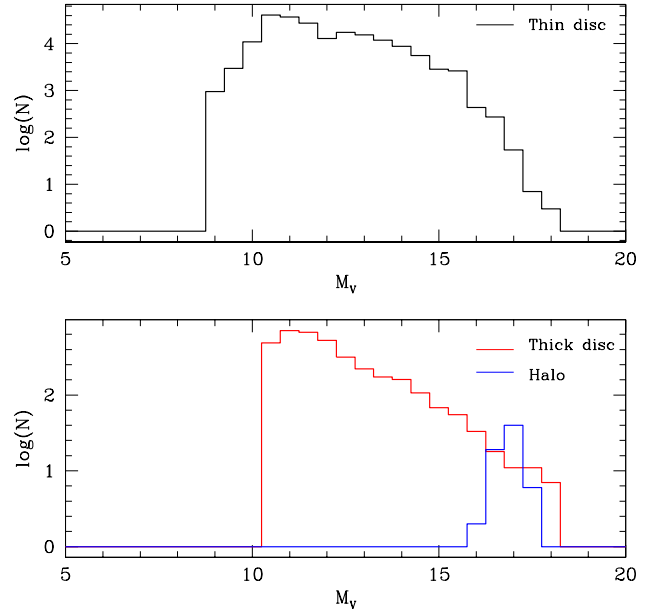In addition to this increase in the number of cool WDs, one of the main contributions of the *Gaia* mission will also be the large portion of sources with good parallaxes (see Table 2 for estimates of the number of WDs observed in all temperature regimes). For cool WDs ($T_{eff} < 5000$ K), GUMS estimates about 2000 with $\frac{\sigma_\pi}{\pi} < 1\%$ (20% of all predicted cool WDs). Furthermore, the complete sample of about 9000 observed cool WDs will have $\frac{\sigma_\pi}{\pi} < 5.5\%$. Table 2 shows that all cool ($T_{eff} < 7000$ K) WDs in the Kilic et al. (2010a) sample extracted from SDSS will have $\frac{\sigma_\pi}{\pi} < 5\%$ when observed with *Gaia*.

The resulting WDs $M_V$ distributions are plotted in Figs. 14 and 15 for Napiwotzki (2009) and GUMS simulations, respectively. Values higher than average $M_V$ are more frequent for thick-disc and halo populations than for thin-disc populations, especially in the Napiwotzki (2009) simulations. These represent the oldest WDs (> 10 Gyr) produced from higher mass progenitors (with much higher masses than the 0.45–0.50 M$_\odot$ WDs that dominate brightness-limited samples of halo WDs). IMFs such as those from Chabrier (1999); Baugh et al. (2005) would enhance these tails resulting in much higher numbers of cool WDs.

Differences in the number of predicted WDs can also be seen in the $T_{eff}$ and $\log g$ histograms plotted in Fig. 16. In GUMS

there are no halo WDs hotter than about 5000 K because of the type of IMF is assumed with an age of 14 Gyr. Thus, the detection and identification of these old massive WDs with *Gaia* will be extremely helpful to obtain information about the IMF of the Galaxy. The peak of the $T_{eff}$ distribution for Napiwotzki (2009) shown in Fig. 16 (top) is centred around 12 000 K, which is the result of the interplay between the WD cooling rate and the change of absolute brightness with temperature.

The present version of GUMS considers only discrete values for $\log g$ (from 7.0 to 9.0 in steps of 0.5). In particular, for the thick-disc and halo WDs only $\log g = 8.0$ was assumed (see Fig. 16). In the simulations of Napiwotzki (2009), the peak tends to be lower for the thick-disc and halo populations than for the thin disc. This agrees with the results obtained by the SPY project (Pauli et al. 2006), showing that hot WDs ($T_{eff} > 10\,000$ K) that belongs to the halo population have masses in the range 0.45–0.50 M$_\odot$.

The predicted HR diagram in *Gaia* observables is shown in Fig. 17. According to Fig. 18 in Robin et al. (2012), the low-mass MS can be perfectly separated from the WD branch (at least for $T_{eff} > 3000$ K). Therefore, we will be able to separate cool WDs from cool MS stars in the *Gaia* catalogues.

We did not aim to discuss which of the two simulations considered here better reproduces the reality, but only to provide an estimate of the number of WDs in different stellar populations predicted to be observed by *Gaia*. On the other hand, a comparison of the true *Gaia* data with our simulations will improve our knowledge about the Milky Way formation and validate the models and assumptions.

## 7. Summary and conclusions

We have presented colour-colour photometric transformations between *Gaia* and other common optical and IR photometric systems (Johnson-Cousins, SDSS and 2MASS) for the case of WDs. To compute these transformations the most recent *Gaia* passbands and WD SED synthetic libraries (Tremblay et al. 2011; Bergeron et al. 2011) were used.
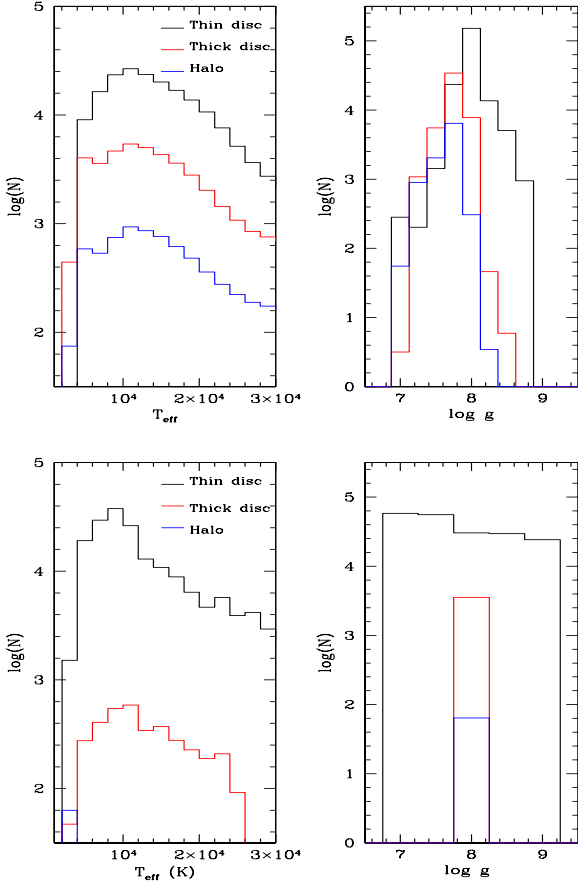
**Fig. 16.** Comparison of $T_{eff}$ and $\log g$ histograms for single WDs in thin-disc, thick-disc, and halo populations obtained using Napiwotzki 2009 (upper panels) and GUMS simulations (bottom panels). GUMS halo and thick-disc WDs are assumed to have $\log g = 8.0$.



**Fig. 17.** Hertzsprung–Russell diagram built using only *Gaia* observable quantities ($G$, $G_{BP}$, $G_{RP}$, and parallaxes) for single WDs with $G \leq 20$ obtained from Napiwotzki (2009), top, and GUMS, bottom. The Hertzsprung–Russell GUMS diagram considers discrete values for $\log g$, which is reflected as quantised trends in this plot. SDSS WD samples extracted from Tremblay et al. (2011) and Kilic et al. (2010a) are overplotted with error bars as expected from *Gaia* observations. Table 2 shows that almost all SDSS WD plotted here have relative error of parallaxes better than 10%.

Two different behaviours were observed depending on the WD effective temperature. In the 'normal' regime ($T_{eff} > 5000$ K) all WDs with the same composition (pure-H or pure-He)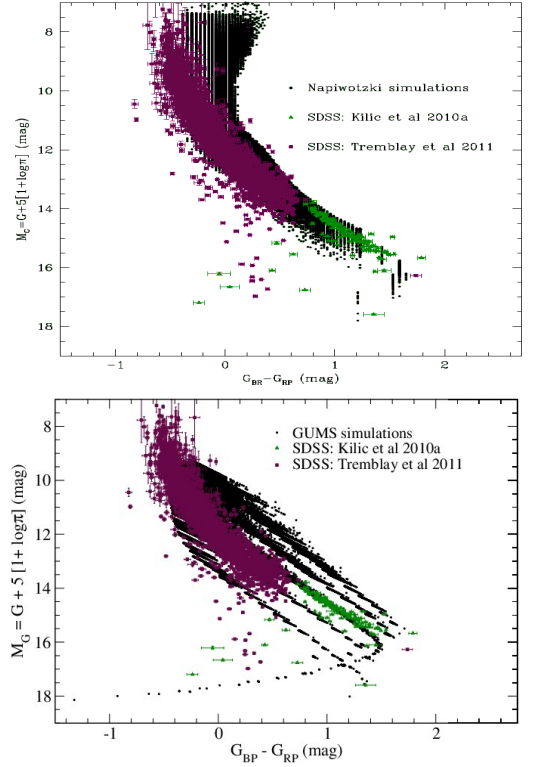 could be fitted by a single law to transform colours into the *Gaia* photometric system. For the very cool regime, WDs with different compositions, $T_{eff}$ and $\log g$, fall in different positions in colour-colour diagram which produces a spread in these diagrams. Colours with blue/UV information, like the *B* Johnson passband, seem to better distinguish the different WD characteristics, but the measurements in this regime will be rather noisy because of the low photon counts for very cool sources and in practice might be hard to use. We therefore expect that observations in near-IR passbands, combined with *Gaia* data, might be very helpful in characterising WDs, especially in the cool regime.

Estimates of the number of WDs that *Gaia* is expected to observe during its five-year mission and the expected precision in parallax were also provided. According to the number of sources predicted by Napiwotzki (2009) and by the *Gaia* Universe Model Snapshot (Robin et al. 2012), we expect between 250 000 and 500 000 WDs detected by *Gaia*. A few thousand of them will have $T_{eff} < 5000$ K, which will increase the statistics of these very cool WDs quite substantially, a regime in which only very few objects have been observed until now (Catalán et al. 2012; Harris et al. 2006).

*Gaia* parallaxes will be extremely important for the identification and characterisation of WDs. We provided estimates of the precision in WD parallaxes that *Gaia* will derive, obtaining that about 95% of WDs will have parallaxes better than 10%. For cool WDs ($T_{eff} < 5000$ K) they will have parallaxes better than 5%, and about 2000 of them will have parallaxes better than 1%.

Additional photometry or/and spectroscopic follow-up might be necessary to achieve a better accuracy on the atmospheric parameters. A comparison of the masses obtained from the *Gaia* parallaxes with those determined from spectroscopic fits will allow testing the mass-radius relations for WDs. A better characterisation of the coolest WDs will also be possible since it will help to resolve the discrepancy regarding the H/He atmospheric composition of these WDs that exist in the literature (Kowalski & Saumon 2006; Kilic et al. 2009b, 2010a). In addition,, the orbital solutions derived for the WDs detected in binary systems will provide independent mass determinations for them, and therefore will allow for stringent tests of the atmosphere models. This will improve the stellar population ages derived by means of the WD cosmochronology and our understanding of the stellar evolution.

## References

Arnaboldi, M., Petr-Gotzens, M., Rejkuba, M., et al. 2010, The Messenger, 139, 6
Bailer-Jones, C. A. L., Andrae, R., Arcay, B., et al. 2013, A&A, 559, A74
Baugh, C. M., Lacey, C. G., Frenk, C. S., et al. 2005, MNRAS, 356, 1191
Bergeron, P., Saumon, D., & Wesemael, F. 1995, ApJ, 443, 764
Bergeron, P., Wesemael, F., Dufour, P., et al. 2011, ApJ, 737, 28
Bessell, M. S. 1990, PASP, 102, 1181
Blöcker, T. 1995, A&A, 299, 755
Bohlin, R. C. 2007, in Astronomical Society of the Pacific Conference Series, Vol. 364, The Future of Photometric, Spectrophotometric and Polarimetric Standardization, ed. C. Sterken, 315
Bonnet, R. M., Høg, E., Bernacca, P. L., et al., eds. 1997, ESA Special Publication, Vol. 402, The celebration session of the Hipparcos - Venice '97 symposium.
Catalán, S., Tremblay, P.-E., Pinfield, D. J., et al. 2012, A&A, 546, L3
Chabrier, G. 1999, ApJ, 513, L103
Cohen, M., Wheaton, W. A., & Megeath, S. T. 2003, AJ, 126, 1090
De Gennaro, S., von Hippel, T., Winget, D. E., et al. 2008, AJ, 135, 1
Drimmel, R., Cabrera-Lavers, A., & López-Corredoira, M. 2003, A&A, 409, 205
Durant, M., Kargaltsev, O., Pavlov, G. G., et al. 2012, ApJ, 746, 6
Eisenstein, D. J., Liebert, J., Harris, H. C., et al. 2006, ApJS, 167, 40
Findlay, J. R., Sutherland, W. J., Venemans, B. P., et al. 2012, MNRAS, 419, 3354
Fontaine, G., Brassard, P., & Bergeron, P. 2001, PASP, 113, 409
Fukugita, M., Ichikawa, T., Gunn, J. E., et al. 1996, AJ, 111, 1748
Giammichele, N., Bergeron, P., & Dufour, P. 2012, ApJS, 199, 29
Girardi, L., Bressan, A., Bertelli, G., & Chiosi, C. 2000, A&AS, 141, 371
Hamuy, M., Suntzeff, N. B., Heathcote, S. R., et al. 1994, PASP, 106, 566
Hamuy, M., Walker, A. R., Suntzeff, N. B., et al. 1992, PASP, 104, 533
Harris, H. C., Munn, J. A., Kilic, M., et al. 2006, AJ, 131, 571
Hewett, P. C., Warren, S. J., Leggett, S. K., & Hodgkin, S. T. 2006, MNRAS, 367, 454
Holberg, J. B. & Bergeron, P. 2006, AJ, 132, 1221
Holberg, J. B., Sion, E. M., Oswalt, T., et al. 2008, AJ, 135, 1225
Hu, Q., Wu, C., & Wu, X.-B. 2007, A&A, 466, 627
Iglesias, C. A., Rogers, F. J., & Saumon, D. 2002, ApJ, 569, L111
Isern, J., Garcia-Berro, E., Hernanz, M., Mochkovitch, R., & Torres, S. 1998, ApJ, 503, 239
Isern, J., García-Berro, E., & Salaris, M. 2001, in Astronomical Society of the Pacific Conference Series, Vol. 245, Astrophysical Ages and Times Scales, ed. T. von Hippel, C. Simpson, & N. Manset, 328
Jordi, C., Gebran, M., Carrasco, J. M., et al. 2010, A&A, 523, A48
Katz, D., Cropper, M., Meynadier, F., et al. 2011, in EAS Publications Series, Vol. 45, EAS Publications Series, 189–194
Kilic, M., Kowalski, P. M., Reach, W. T., & von Hippel, T. 2009a, ApJ, 696, 2094
Kilic, M., Kowalski, P. M., & von Hippel, T. 2009b, AJ, 138, 102
Kilic, M., Leggett, S. K., Tremblay, P.-E., et al. 2010a, ApJS, 190, 77
Kilic, M., Munn, J. A., Williams, K. A., et al. 2010b, ApJ, 715, L21
Kleinman, S. J., Kepler, S. O., Koester, D., et al. 2013, ApJS, 204, 5
Kowalski, P. M., Mazevet, S., Saumon, D., & Challacombe, M. 2007, Phys. Rev. B, 76, 075112
Kowalski, P. M. & Saumon, D. 2004, ApJ, 607, 970
Kowalski, P. M. & Saumon, D. 2006, ApJ, 651, L137
Krzesinski, J., Kleinman, S. J., Nitta, A., et al. 2009, A&A, 508, 339
Leggett, S. K., Lodieu, N., Tremblay, P.-E., Bergeron, P., & Nitta, A. 2011, ApJ, 735, 62
Liebert, J. 1980, ARA&A, 18, 363
Liebert, J., Bergeron, P., & Holberg, J. B. 2005, ApJS, 156, 47
Liebert, J., Dahn, C. C., Harris, H. C., & Legget, S. K. 1999, in Astronomical Society of the Pacific Conference Series, Vol. 169, 11th European Workshop on White Dwarfs, ed. S.-E. Solheim & E. G. Meistas, 51
McCook, G. P. & Sion, E. M. 1999, ApJS, 121, 1
Napiwotzki, R. 2009, Journal of Physics Conference Series, 172, 012004
Napiwotzki, R., Christlieb, N., Drechsel, H., et al. 2001, Astronomische Nachrichten, 322, 411
O'Dell, C. R. & Yusef-Zadeh, F. 2000, AJ, 120, 382
Oke, J. B. 1990, AJ, 99, 1621
Oppenheimer, B. R., Hambly, N. C., Digby, A. P., Hodgkin, S. T., & Saumon, D. 2001, Science, 292, 698

Pancino, E., Altavilla, G., Marinoni, S., et al. 2012, ArXiv e-prints
Pauli, E.-M., Napiwotzki, R., Heber, U., Altmann, M., & Odenkirchen, M. 2006, A&A, 447, 173
Perryman, M. A. C., de Boer, K. S., Gilmore, G., et al. 2001, A&A, 369, 339
Prusti, T. 2011, in EAS Publications Series, Vol. 45, EAS Publications Series, 9–14
Rebassa-Mansergas, A., Nebot Gómez-Morán, A., Schreiber, M. R., Girven, J., & Gänsicke, B. T. 2011, MNRAS, 413, 1121
Reylé, C., Robin, A. C., & Crézé, M. 2001, A&A, 378, L53
Robin, A. C., Luri, X., Reylé, C., et al. 2012, A&A, 543, A100
Robin, A. C., Reylé, C., Derrière, S., & Picaud, S. 2003, A&A, 409, 523
Salaris, M., García-Berro, E., Hernanz, M., Isern, J., & Saumon, D. 2000, ApJ, 544, 1036
Salpeter, E. E. 1955, ApJ, 121, 161
Stritzinger, M., Suntzeff, N. B., Hamuy, M., et al. 2005, PASP, 117, 810
Torres, S., García-Berro, E., Isern, J., & Figueras, F. 2005, MNRAS, 360, 1381
Tremblay, P.-E. & Bergeron, P. 2007, ApJ, 657, 1013
Tremblay, P.-E., Bergeron, P., & Gianninas, A. 2011, ApJ, 730, 128
Weidemann, V. 2000, A&A, 363, 647
Westera, P., Lejeune, T., Buser, R., Cuisinier, F., & Bruzual, G. 2002, A&A, 381, 524
Winget, D. E., Hansen, C. J., Liebert, J., et al. 1987, ApJ, 315, L77
Wood, M. A. 1992, ApJ, 386, 539

**Table 3.** *Gaia*, Johnson, 2MASS, and SDSS absolute magnitudes derived for WD SEDs extracted from Tremblay et al. (2011) for pure-H composition WDs. Only the first records are shown. The full table is available at the CDS.

| $T_{\rm eff}$ | $\log g$ | $M/M_\odot$ | $M_{\rm bol}$ | $BC_V$ | $M_U$ | $M_B$ | $M_V$ | $M_{R_C}$ | $M_{I_C}$ | $M_J$ | $M_H$ | $M_{K_S}$ | $M_u$ | $M_g$ | $M_r$ | $M_i$ | $M_z$ | $M_y$ | $M_G$ | $M_{G_{\rm BP}}$ | $M_{G_{\rm BP}}$ | $M_{G_{\rm RVS}}$ | Age |
|---|---|---|---|---|---|---|---|---|---|---|---|---|---|---|---|---|---|---|---|---|---|---|---|
| 1500 | 7.0 | 0.150 | 19.064 | 1.043 | 22.926 | 20.527 | 18.021 | 17.746 | 19.438 | 19.578 | 19.584 | 21.336 | 23.940 | 19.241 | 17.619 | 19.668 | 19.352 | 17.980 | 18.380 | 18.414 | 18.660 | 19.037 | 1.623E+10 |
| 1750 | 7.0 | 0.151 | 18.393 | 0.787 | 22.232 | 20.018 | 17.607 | 17.153 | 18.233 | 18.418 | 18.556 | 19.798 | 23.228 | 18.800 | 17.070 | 18.526 | 18.313 | 17.583 | 17.779 | 17.933 | 17.705 | 17.888 | 1.338E+10 |
| 2000 | 7.0 | 0.151 | 17.812 | 0.524 | 21.626 | 19.588 | 17.288 | 16.687 | 17.240 | 17.456 | 17.705 | 18.621 | 22.599 | 18.437 | 16.673 | 17.580 | 17.441 | 17.273 | 17.275 | 17.575 | 16.924 | 16.946 | 1.078E+10 |
| 2250 | 7.0 | 0.151 | 17.297 | 0.281 | 21.083 | 19.203 | 17.016 | 16.299 | 16.427 | 16.651 | 16.968 | 17.633 | 22.038 | 18.113 | 16.368 | 16.807 | 16.712 | 17.003 | 16.830 | 17.284 | 16.277 | 16.176 | 7.879E+09 |
| 2500 | 7.0 | 0.152 | 16.837 | 0.059 | 20.590 | 18.855 | 16.778 | 15.974 | 15.757 | 15.963 | 16.330 | 16.817 | 21.529 | 17.822 | 16.128 | 16.191 | 16.094 | 16.764 | 16.440 | 17.039 | 15.740 | 15.538 | 5.479E+09 |
| 2750 | 7.0 | 0.152 | 16.420 | -0.136 | 20.123 | 18.526 | 16.556 | 15.696 | 15.220 | 15.353 | 15.742 | 16.103 | 21.046 | 17.546 | 15.922 | 15.710 | 15.578 | 16.541 | 16.099 | 16.816 | 15.297 | 15.019 | 3.943E+09 |
| 3000 | 7.0 | 0.152 | 16.039 | -0.295 | 19.654 | 18.195 | 16.334 | 15.451 | 14.807 | 14.794 | 15.173 | 15.439 | 20.563 | 17.269 | 15.727 | 15.342 | 15.158 | 16.318 | 15.802 | 16.596 | 14.939 | 14.613 | 3.472E+09 |

. . .

**Table 4.** *Gaia*, Johnson-Cousins, 2MASS, and SDSS absolute magnitudes derived for WD SEDs extracted from Bergeron et al. (2011) for pure-He composition WDs. Only the first records are shown. The full table is available at the CDS.

| $T_{\rm eff}$ | $\log g$ | $M/M_\odot$ | $M_{\rm bol}$ | $BC_V$ | $M_U$ | $M_B$ | $M_V$ | $M_{R_C}$ | $M_{I_C}$ | $M_J$ | $M_H$ | $M_{K_S}$ | $M_u$ | $M_g$ | $M_r$ | $M_i$ | $M_z$ | $M_y$ | $M_G$ | $M_{G_{\rm BP}}$ | $M_{G_{\rm RP}}$ | $M_{G_{\rm RVS}}$ | Age |
|---|---|---|---|---|---|---|---|---|---|---|---|---|---|---|---|---|---|---|---|---|---|---|---|
| 3500 | 7.0 | 0.150 | 15.387 | -1.803 | 20.374 | 19.186 | 17.190 | 15.907 | 14.774 | 13.610 | 13.120 | 12.831 | 21.252 | 18.245 | 16.371 | 15.474 | 14.944 | 17.202 | 16.104 | 17.371 | 14.980 | 14.508 | 2.902E+09 |
| 3750 | 7.0 | 0.151 | 15.083 | -1.432 | 19.367 | 18.340 | 16.515 | 15.371 | 14.352 | 13.350 | 12.921 | 12.670 | 20.235 | 17.475 | 15.785 | 15.008 | 14.569 | 16.517 | 15.605 | 16.720 | 14.546 | 14.114 | 2.792E+09 |
| 4000 | 7.0 | 0.151 | 14.797 | -1.115 | 18.449 | 17.573 | 15.912 | 14.895 | 13.983 | 13.124 | 12.748 | 12.527 | 19.308 | 16.779 | 15.264 | 14.600 | 14.243 | 15.906 | 15.155 | 16.134 | 14.164 | 13.772 | 2.489E+09 |
| 4250 | 7.0 | 0.152 | 14.526 | -0.845 | 17.605 | 16.874 | 15.371 | 14.473 | 13.662 | 12.928 | 12.596 | 12.402 | 18.455 | 16.148 | 14.804 | 14.244 | 13.960 | 15.360 | 14.750 | 15.604 | 13.829 | 13.475 | 2.193E+09 |
| 4500 | 7.0 | 0.153 | 14.271 | -0.617 | 16.818 | 16.233 | 14.888 | 14.100 | 13.384 | 12.758 | 12.464 | 12.293 | 17.662 | 15.575 | 14.398 | 13.934 | 13.715 | 14.872 | 14.384 | 15.125 | 13.535 | 13.218 | 1.955E+09 |
| 4750 | 7.0 | 0.155 | 14.026 | -0.431 | 16.079 | 15.644 | 14.457 | 13.772 | 13.142 | 12.611 | 12.349 | 12.197 | 16.916 | 15.053 | 14.040 | 13.664 | 13.502 | 14.438 | 14.054 | 14.691 | 13.278 | 12.995 | 1.737E+09 |
| 5000 | 7.0 | 0.157 | 13.791 | -0.286 | 15.385 | 15.108 | 14.077 | 13.484 | 12.932 | 12.480 | 12.245 | 12.110 | 16.215 | 14.584 | 13.728 | 13.430 | 13.317 | 14.058 | 13.757 | 14.300 | 13.055 | 12.802 | 1.546E+09 |

. . .

**Table 5.** *Gaia*, Johnson-Cousins, 2MASS, and SDSS absolute magnitudes derived for WD SEDs extracted from Kilic et al. (2010a) for mixed (He/H= 0.1) composition WDs. Only the first records are shown. The full table is available at the CDS.

| $T_{\rm eff}$ | $\log g$ | $M/M_\odot$ | $M_{\rm bol}$ | $BC_V$ | $M_U$ | $M_B$ | $M_V$ | $M_{R_C}$ | $M_{I_C}$ | $M_J$ | $M_H$ | $M_{K_S}$ | $M_u$ | $M_g$ | $M_r$ | $M_i$ | $M_z$ | $M_y$ | $M_G$ | $M_{G_{BP}}$ | $M_{G_{RP}}$ | $M_{G_{RVS}}$ | Age |
|---|---|---|---|---|---|---|---|---|---|---|---|---|---|---|---|---|---|---|---|---|---|---|---|
| 2000 | 7.0 | 0.147 | 17.840 | 1.023 | 18.395 | 17.917 | 16.817 | 17.047 | 18.728 | 19.978 | 21.054 | 23.900 | 19.233 | 17.308 | 16.982 | 18.455 | 19.574 | 16.741 | 17.307 | 17.207 | 18.037 | 19.059 | 1.017E+10 |
| 2250 | 7.0 | 0.147 | 17.331 | 0.894 | 17.960 | 17.561 | 16.437 | 16.392 | 17.764 | 18.949 | 20.028 | 22.339 | 18.794 | 16.974 | 16.351 | 17.550 | 18.563 | 16.387 | 16.771 | 16.762 | 17.113 | 18.016 | 9.629E+09 |
| 2500 | 7.0 | 0.147 | 16.874 | 0.749 | 17.566 | 17.239 | 16.125 | 15.870 | 16.862 | 18.002 | 19.086 | 20.968 | 18.398 | 16.674 | 15.886 | 16.675 | 17.649 | 16.091 | 16.299 | 16.400 | 16.323 | 17.096 | 8.280E+09 |
| 2750 | 7.0 | 0.147 | 16.454 | 0.598 | 17.206 | 16.944 | 15.856 | 15.449 | 16.008 | 17.115 | 18.183 | 19.570 | 18.036 | 16.399 | 15.535 | 15.927 | 16.830 | 15.832 | 15.880 | 16.100 | 15.664 | 16.262 | 4.873E+09 |
| 3000 | 7.0 | 0.148 | 16.068 | 0.441 | 16.884 | 16.681 | 15.627 | 15.126 | 15.300 | 16.357 | 17.403 | 18.354 | 17.712 | 16.156 | 15.270 | 15.379 | 16.057 | 15.608 | 15.530 | 15.852 | 15.140 | 15.484 | 3.673E+09 |
| 3250 | 7.0 | 0.149 | 15.714 | 0.285 | 16.597 | 16.447 | 15.429 | 14.872 | 14.738 | 15.670 | 16.713 | 17.425 | 17.424 | 15.939 | 15.062 | 14.974 | 15.389 | 15.411 | 15.234 | 15.643 | 14.715 | 14.816 | 3.173E+09 |
| 3500 | 7.0 | 0.150 | 15.387 | 0.148 | 16.321 | 16.221 | 15.239 | 14.655 | 14.312 | 15.009 | 16.031 | 16.564 | 17.146 | 15.730 | 14.876 | 14.667 | 14.861 | 15.223 | 14.977 | 15.446 | 14.371 | 14.299 | 2.90E+09 |

. . .

**Table 6.** Coefficients of the colour-colour polynomial fittings using the Johnson-Cousins and SDSS passbands.

| Johnson-Cousins | | | | | | SDSS | | | | | |
|---|---|---|---|---|---|---|---|---|---|---|---|
| **Pure-H ($T_{eff} > 5000$ K)** | | | | | | | | | | | |
| Colour | Zero point | $V-I_C$ | $(V-I_C)^2$ | $(V-I_C)^3$ | $\sigma$ | Colour | Zero point | $g-i$ | $(g-i)^2$ | $(g-i)^3$ | $\sigma$ |
| $G-G_{BP}$ | -0.0106 | -0.4093 | 0.3189 | -0.3699 | 0.009 | $G-G_{BP}$ | -0.1186 | -0.3188 | -0.0276 | -0.0390 | 0.007 |
| $G-G_{RP}$ | 0.0187 | 0.7797 | -0.4716 | 0.3166 | 0.009 | $G-G_{RP}$ | 0.2214 | 0.5655 | -0.0756 | -0.0596 | 0.008 |
| $G-G_{RVS}$ | 0.0517 | 1.0443 | -0.6142 | 0.4035 | 0.013 | $G-G_{RVS}$ | 0.3246 | 0.7604 | -0.1031 | -0.0871 | 0.009 |
| $G_{BP}-G_{RP}$ | 0.0292 | 1.1890 | -0.7905 | 0.6865 | 0.019 | $G_{BP}-G_{RP}$ | 0.3400 | 0.8843 | -0.0480 | -0.0206 | 0.013 |
| $G-V$ | 0.0495 | -0.0907 | -0.6233 | 0.4240 | 0.013 | $G-g$ | -0.1020 | -0.5132 | -0.0980 | -0.0077 | 0.003 |
| $V-G_{RVS}$ | 0.0022 | 1.1350 | 0.0091 | -0.0205 | 0.001 | $g-G_{RVS}$ | 0.4266 | 1.2736 | -0.0051 | -0.0794 | 0.007 |
| $V-G_{BP}$ | -0.0601 | -0.3186 | 0.9421 | -0.7939 | 0.021 | $g-G_{BP}$ | -0.0166 | 0.1943 | 0.0704 | -0.0313 | 0.009 |
| $V-G_{RP}$ | -0.0308 | 0.8704 | 0.1516 | -0.1073 | 0.004 | $g-G_{RP}$ | 0.3234 | 1.0787 | 0.0224 | -0.0519 | 0.005 |
| Color | Zero point | $V-R$ | $(V-R)^2$ | $(V-R)^3$ | $\sigma$ | Colour | Zero point | $g-r$ | $(g-r)^2$ | $(g-r)^3$ | $\sigma$ |
| $G-G_{BP}$ | -0.0232 | -0.9322 | 1.9936 | -3.8732 | 0.015 | $G-G_{BP}$ | -0.0891 | -0.5172 | -0.0306 | -0.0206 | 0.007 |
| $G-G_{RP}$ | 0.0427 | 1.7388 | -3.2195 | 4.3387 | 0.019 | $G-G_{RP}$ | 0.1658 | 0.9376 | -0.1314 | -0.3685 | 0.011 |
| $G-G_{RVS}$ | 0.0838 | 2.3270 | -4.2247 | 5.6185 | 0.026 | $G-G_{RVS}$ | 0.2498 | 1.2602 | -0.1749 | -0.5183 | 0.014 |
| $G_{BP}-G_{RP}$ | 0.0659 | 2.6710 | -5.2132 | 8.2118 | 0.034 | $G_{BP}-G_{RP}$ | 0.2550 | 1.4548 | -0.1008 | -0.3480 | 0.016 |
| $G-V$ | 0.0473 | -0.1712 | -2.8314 | 4.0591 | 0.017 | $G-g$ | -0.0555 | -0.8062 | -0.2123 | 0.1398 | 0.003 |
| $V-G_{RVS}$ | 0.0366 | 2.4982 | -1.3933 | 1.5594 | 0.010 | $g-G_{RVS}$ | 0.3053 | 2.0664 | 0.0374 | -0.6581 | 0.015 |
| $V-G_{BP}$ | -0.0704 | -0.7610 | 4.8250 | -7.9323 | 0.032 | $g-G_{BP}$ | -0.0336 | 0.2889 | 0.1817 | -0.1604 | 0.009 |
| $V-G_{RP}$ | -0.0045 | 1.9100 | -0.3881 | 0.2796 | 0.003 | $g-G_{RP}$ | 0.2214 | 1.7438 | 0.0809 | -0.5083 | 0.011 |
| Colour | Zero point | $R-I$ | $(R-I)^2$ | $(R-I)^3$ | $\sigma$ | Colour | Zero point | $r-i$ | $(r-i)^2$ | $(r-i)^3$ | $\sigma$ |
| $G-G_{BP}$ | 0.0002 | -0.7288 | 0.7736 | -2.3657 | 0.007 | $G-G_{BP}$ | -0.1647 | -0.8976 | -0.9866 | -2.5767 | 0.008 |
| $G-G_{RP}$ | -0.0015 | 1.4227 | -0.9942 | 1.4162 | 0.006 | $G-G_{RP}$ | 0.3038 | 1.4093 | -0.2031 | 0.8241 | 0.008 |
| $G-G_{RVS}$ | 0.0247 | 1.9071 | -1.2742 | 1.7530 | 0.007 | $G-G_{RVS}$ | 0.4355 | 1.8921 | -0.3275 | 0.9117 | 0.008 |
| $G_{BP}-G_{RP}$ | -0.0017 | 2.1515 | -1.7679 | 3.7820 | 0.013 | $G_{BP}-G_{RP}$ | 0.4685 | 2.3069 | 0.7835 | 3.4008 | 0.015 |
| $G-V$ | 0.0509 | -0.1835 | -2.1595 | 2.7057 | 0.010 | $G-g$ | -0.1796 | -1.5031 | -1.6721 | -2.4821 | 0.009 |
| $V-G_{RVS}$ | -0.0262 | 2.0906 | 0.8853 | -0.9527 | 0.007 | $g-G_{RVS}$ | 0.6150 | 3.3952 | 1.3446 | 3.3938 | 0.012 |
| $V-G_{BP}$ | -0.0507 | -0.5453 | 2.9331 | -5.0714 | 0.015 | $g-G_{BP}$ | 0.0149 | 0.6055 | 0.6855 | -0.0945 | 0.010 |
| $V-G_{RP}$ | -0.0524 | 1.6062 | 1.1653 | -1.2894 | 0.009 | $g-G_{RP}$ | 0.4834 | 2.9124 | 1.4690 | 3.3062 | 0.012 |
| Colour | Zero point | $B-V$ | $(B-V)^2$ | $(B-V)^3$ | $\sigma$ | Colour | Zero point | $g-z$ | $(g-z)^2$ | $(g-z)^3$ | $\sigma$ |
| $G-G_{BP}$ | 0.0700 | -0.5674 | -0.4765 | 0.4891 | 0.015 | $G-G_{BP}$ | -0.1488 | -0.2450 | -0.0313 | -0.0325 | 0.006 |
| $G-G_{RP}$ | -0.1251 | 1.0288 | 0.8762 | -1.2221 | 0.033 | $G-G_{RP}$ | 0.2756 | 0.4128 | -0.0513 | -0.0099 | 0.004 |
| $G-G_{RVS}$ | -0.1404 | 1.3779 | 1.1891 | -1.6605 | 0.044 | $G-G_{RVS}$ | 0.3973 | 0.5549 | -0.0713 | -0.0170 | 0.004 |
| $G_{BP}-G_{RP}$ | -0.1951 | 1.5962 | 1.3527 | -1.7112 | 0.047 | $G_{BP}-G_{RP}$ | 0.4244 | 0.6579 | -0.0201 | 0.0226 | 0.008 |
| $G-V$ | 0.0607 | -0.1378 | -0.8979 | 0.7349 | 0.020 | $G-g$ | -0.1508 | -0.4044 | -0.0731 | -0.0219 | 0.006 |
| $V-G_{RVS}$ | -0.2011 | 1.5157 | 2.0870 | -2.3954 | 0.063 | $g-G_{RVS}$ | 0.5481 | 0.9593 | 0.0018 | 0.0049 | 0.002 |
| $V-G_{BP}$ | 0.0093 | -0.4297 | 0.4214 | -0.2458 | 0.006 | $g-G_{BP}$ | 0.0020 | 0.1594 | 0.0418 | -0.0106 | 0.010 |
| $V-G_{RP}$ | -0.1858 | 1.1666 | 1.7741 | -1.9570 | 0.052 | $g-G_{RP}$ | 0.4264 | 0.8173 | 0.0217 | 0.0120 | 0.003 |
| **Pure-He (All $T_{eff}$)** | | | | | | | | | | | |
| Colour | Zero point | $V-I_C$ | $(V-I_C)^2$ | $(V-I_C)^3$ | $\sigma$ | Colour | Zero point | $g-i$ | $(g-i)^2$ | $(g-i)^3$ | $\sigma$ |
| $G-G_{BP}$ | 0.0372 | -0.4155 | -0.0864 | 0.0149 | 0.005 | $G-G_{BP}$ | -0.1127 | -0.3463 | -0.0320 | 0.0028 | 0.004 |
| $G-G_{RP}$ | -0.0166 | 0.7803 | -0.1451 | 0.0067 | 0.004 | $G-G_{RP}$ | 0.2307 | 0.5106 | -0.0860 | 0.0063 | 0.004 |
| $G-G_{RVS}$ | -0.0076 | 1.0204 | -0.1584 | 0.0035 | 0.006 | $G-G_{RVS}$ | 0.3194 | 0.6817 | -0.0984 | 0.0063 | 0.008 |
| $G_{BP}-G_{RP}$ | -0.0538 | 1.1958 | -0.0587 | -0.0082 | 0.009 | $G_{BP}-G_{RP}$ | 0.3434 | 0.8568 | -0.0539 | 0.0034 | 0.007 |
| $G-V$ | -0.0085 | -0.1051 | -0.1541 | 0.0046 | 0.006 | $G-g$ | -0.1051 | -0.5219 | -0.0949 | 0.0065 | 0.001 |
| $V-G_{RVS}$ | 0.0009 | 1.1255 | -0.0043 | -0.0011 | 0.002 | $g-G_{RVS}$ | 0.4244 | 1.2036 | -0.0035 | -0.0002 | 0.007 |
| $V-G_{BP}$ | 0.0456 | -0.3104 | 0.0676 | 0.0103 | 0.010 | $g-G_{BP}$ | -0.0076 | 0.1756 | 0.0629 | -0.0036 | 0.004 |
| $V-G_{RP}$ | -0.0082 | 0.8854 | 0.0089 | 0.0021 | 0.003 | $g-G_{RP}$ | 0.3358 | 1.0324 | 0.0090 | -0.0002 | 0.003 |
| Colour | Zero point | $V-R$ | $(V-R)^2$ | $(V-R)^3$ | $\sigma$ | Colour | Zero point | $g-r$ | $(g-r)^2$ | $(g-r)^3$ | $\sigma$ |
| $G-G_{BP}$ | 0.0410 | -0.8360 | -0.3441 | 0.1642 | 0.006 | $G-G_{BP}$ | -0.0758 | -0.5153 | -0.0698 | 0.0054 | 0.007 |
| $G-G_{RP}$ | -0.0238 | 1.5787 | -0.6202 | 0.0600 | 0.010 | $G-G_{RP}$ | 0.1743 | 0.8064 | -0.2102 | 0.0258 | 0.007 |
| $G-G_{RVS}$ | -0.0169 | 2.0629 | -0.6808 | 0.0292 | 0.015 | $G-G_{RVS}$ | 0.2443 | 1.0710 | -0.2412 | 0.0271 | 0.012 |
| $G_{BP}-G_{RP}$ | -0.0647 | 2.4147 | -0.2761 | -0.1042 | 0.016 | $G_{BP}-G_{RP}$ | 0.2501 | 1.3217 | -0.1403 | 0.0204 | 0.013 |
| $G-V$ | -0.0073 | -0.2094 | -0.6447 | 0.1165 | 0.006 | $G-g$ | -0.0500 | -0.7598 | -0.2141 | 0.0145 | 0.006 |
| $V-G_{RVS}$ | -0.0096 | 2.2723 | -0.0361 | -0.0873 | 0.013 | $g-G_{RVS}$ | 0.2943 | 1.8309 | -0.0271 | 0.0126 | 0.018 |
| $V-G_{BP}$ | 0.0483 | -0.6266 | 0.3006 | 0.0477 | 0.012 | $g-G_{BP}$ | -0.0258 | 0.2446 | 0.1443 | -0.0091 | 0.003 |
| $V-G_{RP}$ | -0.0164 | 1.7881 | 0.0245 | -0.0565 | 0.008 | $g-G_{RP}$ | 0.2243 | 1.5662 | 0.0039 | 0.0113 | 0.013 |
| Colour | Zero point | $R-I$ | $(R-I)^2$ | $(R-I)^3$ | $\sigma$ | Colour | Zero point | $r-i$ | $(r-i)^2$ | $(r-i)^3$ | $\sigma$ |
| $G-G_{BP}$ | 0.0334 | -0.8238 | -0.3379 | 0.0480 | 0.008 | $G-G_{BP}$ | -0.1866 | -1.0602 | -0.2816 | 0.1400 | 0.006 |
| $G-G_{RP}$ | -0.0104 | 1.5351 | -0.5160 | 0.0353 | 0.007 | $G-G_{RP}$ | 0.3332 | 1.3942 | -0.6660 | 0.0952 | 0.006 |
| $G-G_{RVS}$ | 0.0007 | 2.0093 | -0.5587 | 0.0195 | 0.007 | $G-G_{RVS}$ | 0.4570 | 1.8812 | -0.7615 | 0.0749 | 0.007 |
| $G_{BP}-G_{RP}$ | -0.0438 | 2.3589 | -0.1781 | -0.0127 | 0.015 | $G_{BP}-G_{RP}$ | 0.5198 | 2.4544 | -0.3844 | -0.0449 | 0.012 |
| $G-V$ | -0.0101 | -0.2112 | -0.5643 | -0.0837 | 0.008 | $G-g$ | -0.2192 | -1.6588 | -0.8081 | 0.2847 | 0.014 |
| $V-G_{RVS}$ | 0.0107 | 2.2205 | 0.0056 | 0.1033 | 0.012 | $g-G_{RVS}$ | 0.6762 | 3.5400 | 0.0466 | -0.2098 | 0.016 |
| $V-G_{BP}$ | 0.0434 | -0.6126 | 0.2264 | 0.1317 | 0.009 | $g-G_{BP}$ | 0.0326 | 0.5986 | 0.5265 | -0.1447 | 0.009 |
| $V-G_{RP}$ | -0.0004 | 1.7463 | 0.0483 | 0.1190 | 0.013 | $g-G_{RP}$ | 0.5524 | 3.0530 | 0.1421 | -0.1895 | 0.017 |
| Colour | Zero point | $B-V$ | $(B-V)^2$ | $(B-V)^3$ | $\sigma$ | Colour | Zero point | $g-z$ | $(g-z)^2$ | $(g-z)^3$ | $\sigma$ |
| $G-G_{BP}$ | 0.0247 | -0.5733 | 0.0044 | -0.0178 | 0.012 | $G-G_{BP}$ | -0.1499 | -0.2838 | -0.0201 | 0.0012 | 0.002 |
| $G-G_{RP}$ | -0.0008 | 1.0490 | -0.4004 | 0.0790 | 0.017 | $G-G_{RP}$ | 0.2843 | 0.3961 | -0.0547 | 0.0035 | 0.002 |
| $G-G_{RVS}$ | 0.0140 | 1.3753 | -0.4842 | 0.0958 | 0.024 | $G-G_{RVS}$ | 0.3910 | 0.5316 | -0.0628 | 0.0036 | 0.005 |
| $G_{BP}-G_{RP}$ | -0.0255 | 1.6223 | -0.4048 | 0.0967 | 0.028 | $G_{BP}-G_{RP}$ | 0.4342 | 0.6800 | -0.0346 | 0.0023 | 0.003 |
| $G-V$ | -0.0145 | -0.1528 | -0.1763 | -0.0046 | 0.014 | $G-g$ | -0.1616 | -0.4358 | -0.0603 | 0.0030 | 0.007 |
| $V-G_{RVS}$ | 0.0285 | 1.5281 | -0.3080 | 0.1004 | 0.038 | $g-G_{RVS}$ | 0.5526 | 0.9674 | -0.0025 | 0.0006 | 0.003 |
| $V-G_{BP}$ | 0.0392 | -0.4205 | 0.1807 | -0.0131 | 0.003 | $g-G_{BP}$ | 0.0117 | 0.1520 | 0.0402 | -0.0018 | 0.007 |
| $V-G_{RP}$ | 0.0137 | 1.2018 | -0.2241 | 0.0836 | 0.030 | $g-G_{RP}$ | 0.4459 | 0.8320 | 0.0056 | 0.0005 | 0.005 |

**Table 7.** Coefficients of the colour-colour polynomial fittings using 2MASS passbands.

| Colour | Zero point | $J - H$ | $(J - H)^2$ | $(J - H)^3$ | $\sigma$ |
|---|---|---|---|---|---|
| **Pure-H (with $T_{\text{eff}} > 5000$ K)** | | | | | |
| $G-G_{\text{BP}}$ | -0.0034 | -1.1932 | 2.1269 | -8.0313 | 0.028 |
| $G-G_{\text{RP}}$ | 0.0065 | 2.2502 | -3.2057 | 6.3488 | 0.029 |
| $G-G_{\text{RVS}}$ | 0.0356 | 3.0105 | -4.1872 | 8.1704 | 0.037 |
| $G_{\text{BP}}$-$G_{\text{RP}}$ | 0.0099 | 3.4434 | -5.3326 | 14.3800 | 0.056 |
| $G - J$ | -0.1012 | 4.6781 | -5.8656 | 12.5043 | 0.062 |
| $G - H$ | -0.1012 | 5.6781 | -5.8656 | 12.5043 | 0.062 |
| $G - K_S$ | -0.1471 | 6.0017 | -6.5462 | 15.6901 | 0.068 |

| Colour | Zero point | $H - K_S$ | $(H - K_S)^2$ | $(H - K_S)^3$ | $\sigma$ |
|---|---|---|---|---|---|
| $G-G_{\text{BP}}$ | -0.1554 | -3.3439 | 1.7800 | 17.6435 | 0.032 |
| $G-G_{\text{RP}}$ | 0.2713 | 5.4984 | -12.2013 | -88.7226 | 0.050 |
| $G-G_{\text{RVS}}$ | 0.3897 | 7.3579 | -16.1908 | -120.0339 | 0.069 |
| $G_{\text{BP}}$-$G_{\text{RP}}$ | 0.4267 | 8.8424 | -13.9813 | -106.3661 | 0.080 |
| $G - J$ | 0.4739 | 11.9522 | -25.0546 | -216.7318 | 0.090 |
| $G - H$ | 0.6107 | 14.8963 | -28.7366 | -293.7142 | 0.110 |
| $G - K_S$ | 0.6107 | 15.8963 | -28.7366 | -293.7142 | 0.110 |

| Colour | Zero point | $J - H$ | $(J - H)^2$ | $(J - H)^3$ | $\sigma$ |
|---|---|---|---|---|---|
| **Pure-He (All $T_{\text{eff}}$)** | | | | | |
| $G-G_{\text{BP}}$ | -0.0161 | -1.5484 | -1.7352 | 1.0170 | 0.039 |
| $G-G_{\text{RP}}$ | 0.0854 | 2.6145 | -1.1648 | -0.3721 | 0.027 |
| $G-G_{\text{RVS}}$ | 0.1256 | 3.4444 | -1.1064 | -0.6378 | 0.037 |
| $G_{\text{BP}}$-$G_{\text{RP}}$ | 0.1015 | 4.1628 | 0.5704 | -1.3891 | 0.065 |
| $G - J$ | -0.0079 | 5.1327 | -0.1668 | -1.4542 | 0.049 |
| $G - H$ | -0.0079 | 6.1327 | -0.1668 | -1.4542 | 0.049 |
| $G - K_S$ | -0.0304 | 6.7716 | 0.1327 | -1.9867 | 0.047 |

| Colour | Zero point | $H - K_S$ | $(H - K_S)^2$ | $(H - K_S)^3$ | $\sigma$ |
|---|---|---|---|---|---|
| $G-G_{\text{BP}}$ | -0.0661 | -2.5496 | -3.4271 | 3.7898 | 0.046 |
| $G-G_{\text{RP}}$ | 0.1692 | 3.9294 | -4.1881 | 2.2276 | 0.036 |
| $G-G_{\text{RVS}}$ | 0.2360 | 5.2135 | -4.4738 | 2.0733 | 0.049 |
| $G_{\text{BP}}$-$G_{\text{RP}}$ | 0.2354 | 6.4790 | -0.7610 | -1.5622 | 0.080 |
| $G - J$ | 0.1599 | 7.8890 | -3.5933 | 2.1854 | 0.066 |
| $G - H$ | 0.1933 | 9.4216 | -4.3087 | 4.3196 | 0.070 |
| $G - K_S$ | 0.1933 | 10.4216 | -4.3087 | 4.3196 | 0.070 |